Chapter 4: Synthesis and tribological behaviour of vacuum hot press sintered Ni_3Al-based composites containing Ag, WS_2 and Ag-WS_2 at elevated temperature

This chapter begins with the results on the characterization of elemental powders, synthesized Ni_3Al powders, and ball-milled powders, followed by the microstructure and properties (physical and mechanical) evaluation of Ni_3Al-based composites containing either a single solid lubricant or their combinations, i.e., Ni_3Al, Ni_3Al-10 wt.% Ag, Ni_3Al-10 wt.% WS_2, and Ni_3Al-5 wt.% Ag-5 wt.% WS_2 synthesised via vacuum hot press sintering. The chapter also contains the results on the friction and wear test performance of Ni_3Al and the above-mentioned composites. The results have been discussed based on the features seen on the worn surfaces of Ni_3Al-based composites and the counterface Si_3N_4 slid against them to develop an understanding of their tribological behaviour and reveal the prevailing wear mechanisms.

4.1 Results and discussions

4.1.1 Characterization of elemental powders

4.1.1.1 Field emission scanning electron microscopy and XRD of elemental powders

Figure 4.1 shows the FE-SEM morphologies and X-ray diffraction pattern of Ni, Mo, Al, Cr, Zr, B, WS_2, and Ag powders used in the present study. Fig. 4.1(a) illustrates that the Nickel (Ni) powders having a purity of 99.8 % have a dendritic particle shape with particle sizes ranging from 40-50 μm, whereas Al (purity-99.5 %) powder particles are observed to be spherical in shape with particle size ranging from 7-15 μm (Fig. 4.1c). Molybdenum (Mo), Zirconium (Zr), and Boron (B) powder particles exhibited an irregular shape, while Chromium (Cr) powder particles has shown an angular shape, as evident in Figs. 4.1(b, d-f). The particles of WS_2 powder (purity- 99 %) show flower-like morphology with a particle

size of 2 μm, whereas the Ag powder particles (purity- 99 %) have an irregular shape with a particle size of 40-50 μm, as shown in Fig. 4.1(g and h). X-ray diffraction analysis (Figs. 4.1i and j) has shown the presence of Ni, Mo, Al, Cr, Zr, B, WS_2 and Ag powders.

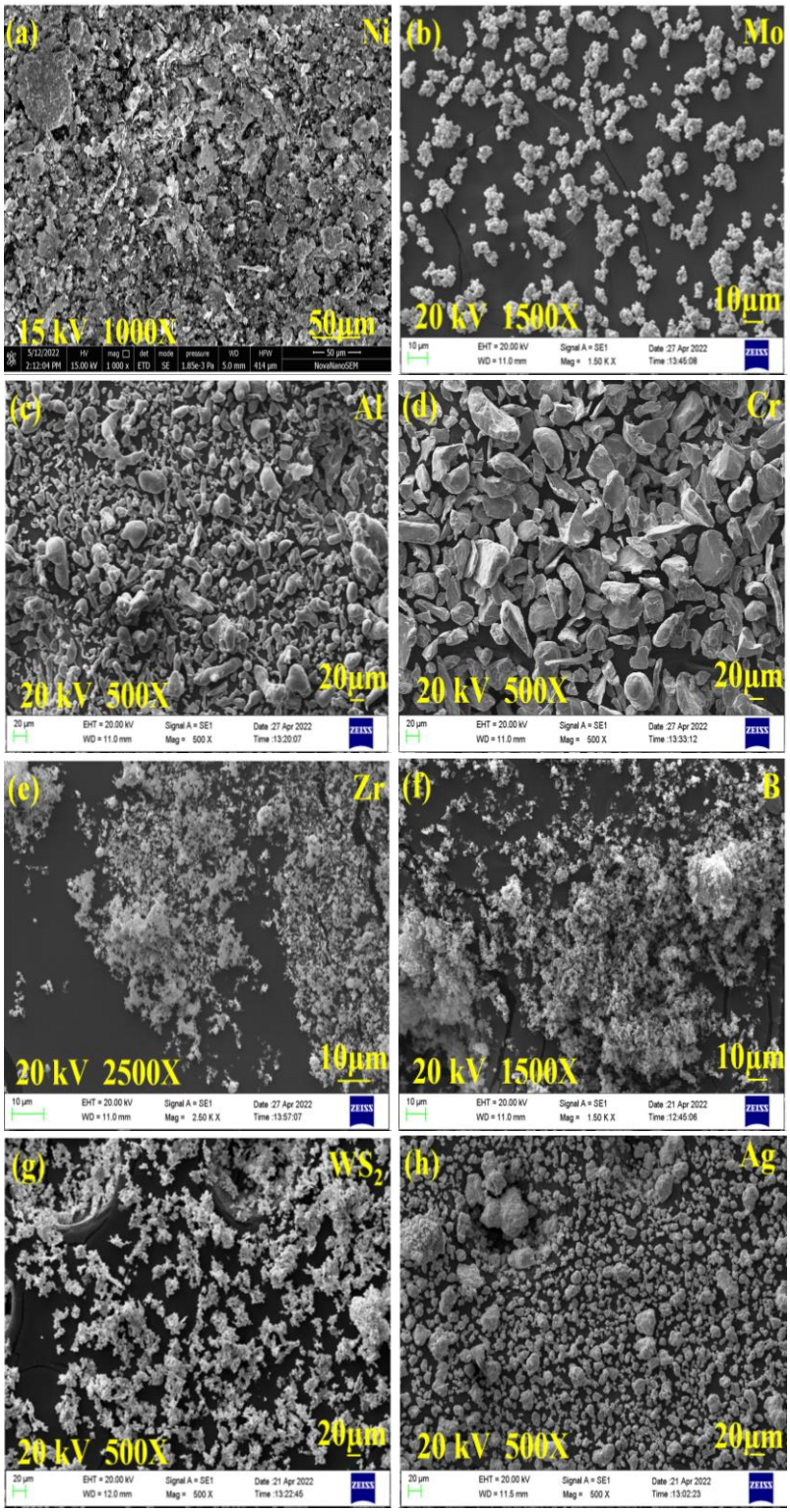

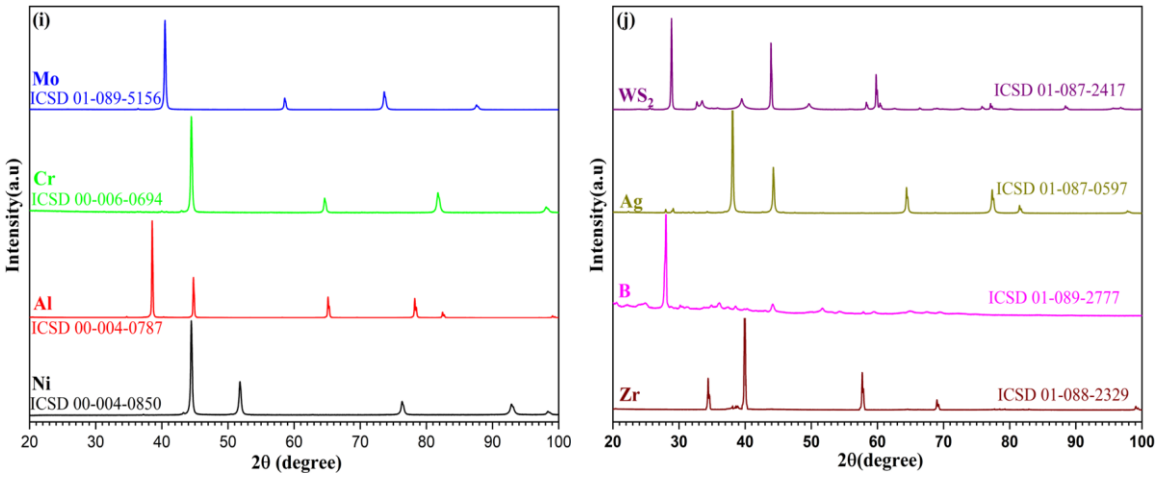

Fig. 4.1: FESEM micrographs of elemental powders: (a) Ni, (b) Mo, (c) Al, (d) Cr, (e) Zr, (f) B, (g) WS_2, (h) Ag, and their XRD analyses (i) and (j).

4.1.2 Characterization of composites

4.1.2.1 FE-SEM and Thermogravimetric analysis of Ball-milled Powders

Figure 4.2(a-d) showcases the FE-SEM micrographs of ball-milled powders of four different compositions: Ni_3Al, Ni_3Al-10Ag, Ni_3Al-10WS_2, and Ni_3Al-5Ag-5WS_2. The micrographs provide valuable insights into the morphological characteristics and structural features of the powders. In Figure 4.2(a), the micrograph of the ball-milled Ni_3Al powder reveals the presence of fine particles with a relatively uniform distribution. The particles appear to have undergone significant deformation and exhibit a moderate level of agglomeration. Figure 4.2(b) displays the micrograph of Ni_3Al-10Ag powder after ball milling. The image shows a similar morphology to that of the Ni_3Al powder, with fine particles and some agglomeration. However, the presence of Ag as an alloying element seems to have influenced the particle size distribution and resulted in a slightly coarser microstructure compared to Ni_3Al alone. The micrograph of ball-milled Ni_3Al-10WS_2 powder (Fig. 4.2c) reveals a distinct change in the morphology compared to the previous two compositions. The powder exhibits a relatively homogeneous distribution of powder particles, possibly attributed to the presence of the WS_2 lubricant. The powder particles

appear to be well-dispersed, suggesting an effective lubricating and reinforcing effect. Figure 4.2(d) shows the micrograph of the ball-milled Ni_3Al-5Ag-5WS_2 powder. This composition combines the addition of both Ag and WS_2. The micrograph reveals a heterogeneous morphology, characterised by the presence of both fine particles and larger agglomerates. The agglomeration may arise due to the mutual interaction between Ag and WS_2, leading to the formation of larger clusters. The particle distribution appears less uniform than the previous compositions, indicating a complex interplay between the two alloying elements.

Figure 4.2 (e) presents the TG curves (mass gain vs. temperature) obtained during the heating of milled powders (Ni_3Al, Ni_3Al-10Ag, Ni_3Al-10WS_2, and Ni_3Al-5Ag-5WS_2) from RT to 800 °C under the flow of N_2 gas. The results show that all of them offer similar TG behaviour below 400 °C, while the weight gain of NI-10W, NI-10AW, NI-10A, and NI has an obvious increase at temperatures above 500 °C. The distinct oxidation processes of NI-10W, NI-10AW, NI-10A, and NI indicate that a chemical reaction related to Ni, Mo, Ag, WS_2, and O_2 might have occurred.

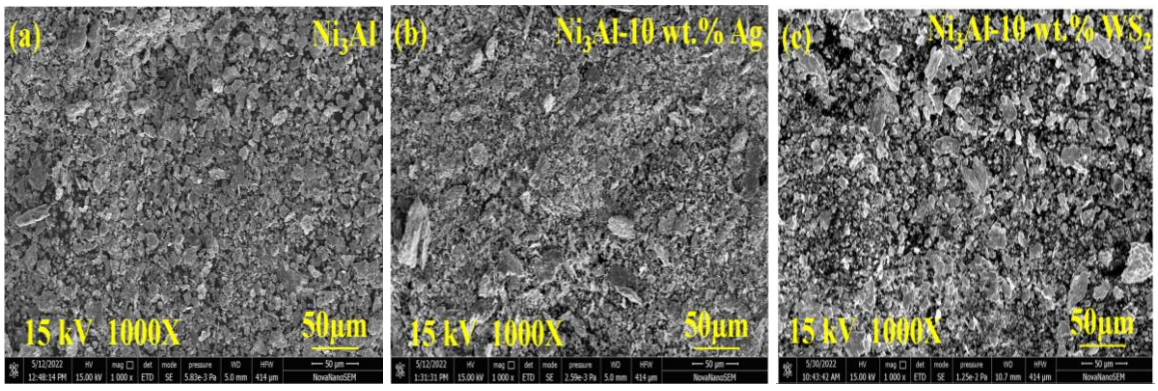

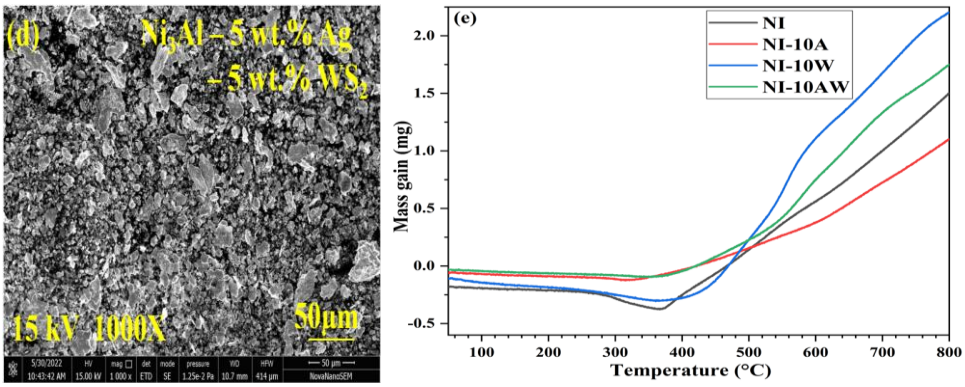

Fig. 4.2: FESEM micrographs of milled powders: (a) Ni_3Al, (b) Ni_3Al-10Ag, (c) Ni_3Al-10WS_2, and (d) Ni_3Al-5Ag-5WS_2, and their thermo-gravimetric analysis (e).

4.1.2.2 X-ray diffraction analysis of ball-milled powders and composites

The diffraction patterns corresponding to milled powders reveal the presence of Ni_3Al (ICSD 03-065-430), Mo (ICSD 01-089-5156), Ag (ICSD 01-087-0597) and WS_2 (ICSD 00-008-0237) as seen from Fig. 4.3 (a) indicating the formation of intermetallic compound Ni_3Al. The X-ray diffraction patterns of NI, NI-10A, NI-10W, and NI-10AW sintered composites illustrated in Fig. 4.3 (b) also demonstrate the presence of intense peaks corresponding to Ni_3Al (ICSD 03-065-430) apart from the peaks of Ag (ICSD 01-087-0598) and WS_2 (ICSD 00-008-0237) which confirms that the powders are sintered under vacuum environment without any oxidation or disintegration.

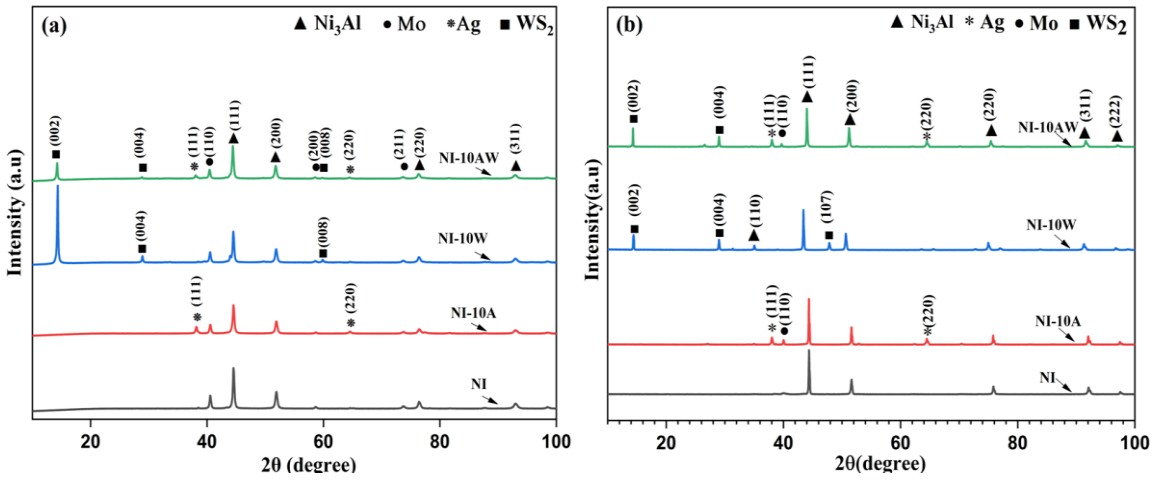

Fig. 4.3: X-ray diffraction patterns of (a) ball milled powder and (b) vacuum hot pressed sintered composite for Ni_3Al, Ni_3Al-10Ag, Ni_3Al-10WS_2, and Ni_3Al-5Ag-5WS_2.

4.1.2.3 Microstructure of composites

The microstructures and elemental mapping of Ni_3Al, Ni_3Al-10Ag, Ni_3Al-10WS_2 and Ni_3Al-5Ag-5WS_2 composites as examined under FESEM are shown in Fig. 4.4. The micrographs show that the vacuum hot-press sintered composites have a dense microstructure with a uniform distribution of all its constituent elements, i.e., presence of Ag in NI-10A (Fig. 4.4b), WS_2 in NI-10W (Fig. 4.4c) and both Ag and WS_2 in NI-10AW (Fig. 4.4d) as marked by the arrows in respective micrographs. The specimen designation, composition, density, and micro-hardness are given in Table 4.1.

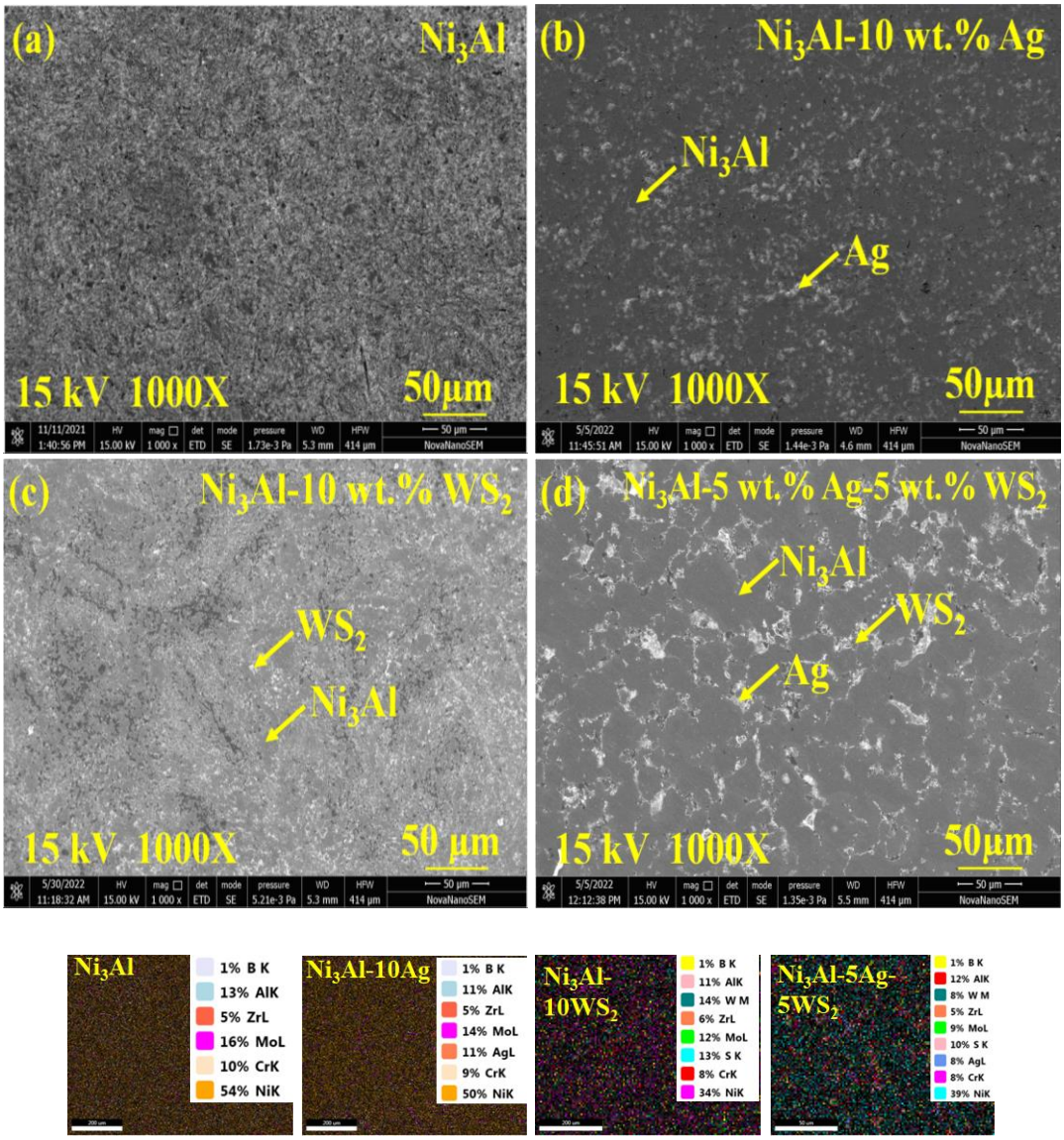

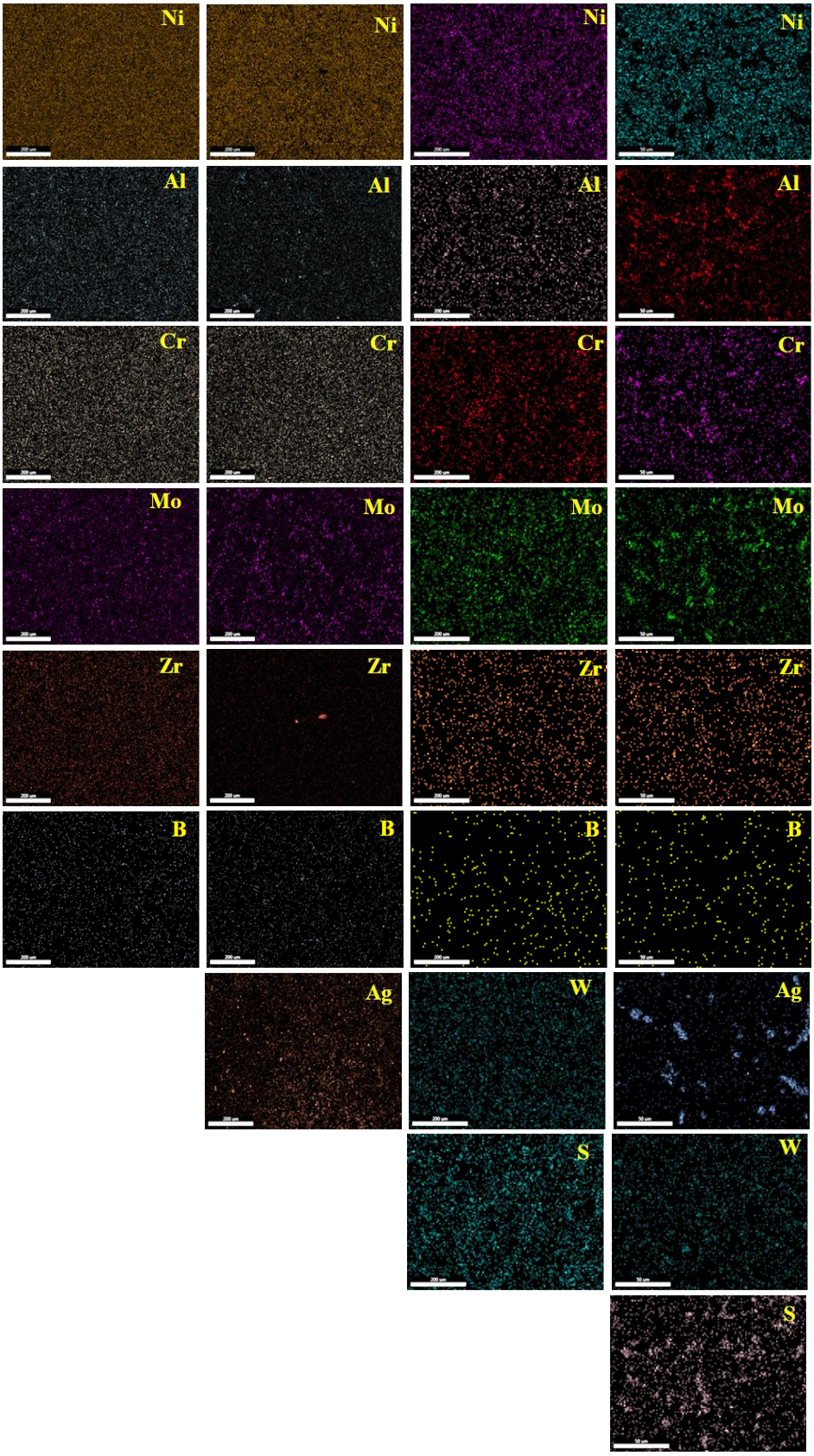

Fig. 4.4: Microstructures of (a) Ni_3Al, (b) Ni_3Al-10Ag, (c) Ni_3Al-10WS_2, and (d) Ni_3Al-5Ag-5WS_2 and corresponding EDS elemental mapping.

4.1.2.4 Hardness and density measurement of composites

One may observe from Fig. 4.5 and Table 4.1 that the hardness of Ni_3Al gets reduced from 355 ± 5 $HV_{0.2}$ to 313 ± 6 $HV_{0.2}$ by the addition of Ag. On the other hand, the addition of WS_2 to the Ni_3Al composite makes it harder, from 355 ± 5 $HV_{0.2}$ to 365 ± 5 $HV_{0.2}$ in Ni_3Al-10WS_2. However, the addition of both Ag and WS_2 to Ni_3Al results in a hardness of 345 ± 8 $HV_{0.2}$.

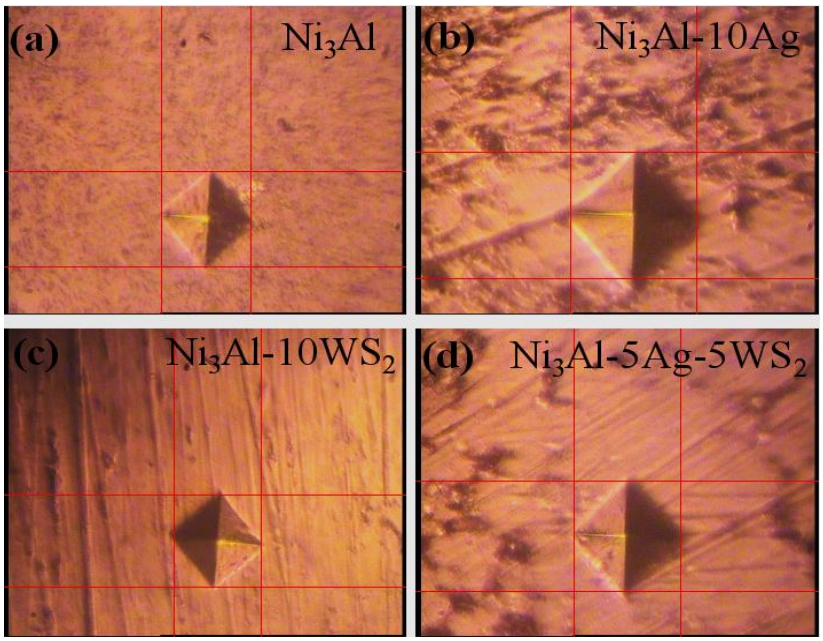

Fig. 4.5: Microhardness (HV) indentation images of (a) Ni_3Al, (b) Ni_3Al-10Ag, (c) Ni_3Al-10WS_2, and (d) Ni_3Al-5Ag-5WS_2.

Table 4.1: Specimen designation, composition, density, and microhardness.

Designation	Composition	Real density (g/cm^3)	Relative density (%)	Microhardness $HV_{0.2}$ (GPa)
NI	100 wt.% Ni_3Al	8.372	99.46	355 ± 5 (3.48)
NI-10A	90 wt.% Ni_3Al-10 wt.% Ag	8.328	96.67	313 ± 6 (3.07)
NI-10W	90 wt.% Ni_3Al-10 wt.% WS_2	8.105	97.42	365 ± 5 (3.58)
NI-10AW	90 wt.% Ni_3Al-5 wt.% Ag- 5 wt.% WS_2	8.395	99.11	345 ± 8 (3.38)

4.1.3 Dry sliding friction and wear behaviour of composites

4.1.3.1 Dry sliding friction

4.1.3.1.1 Variation of coefficient of friction with time

Figures 4.6 (a-e) illustrate the variation of coefficient of friction with time for Ni_3Al, Ni_3Al-10Ag, Ni_3Al-10WS_2 and Ni_3Al-5Ag-5WS_2 composites at RT, 200 °C, 400 °C, 600 °C and 800 °C under a normal load of 10 N and sliding speed of 0.2 m/s. The Ni_3Al composite exhibits a consistently higher coefficient of friction than the composites at all the temperatures, as seen from Fig. 4.6. At room temperature, the coefficient of friction for Ni_3Al appears to stabilise after 200 s and remains constant thereafter till the completion of the test whereas for the NI-10A, NI-10W, and NI-10AW stabilisation seems to occur after an initial run-in duration of 900 s, 300 s, and 1000 s, respectively, with relatively less amplitude of fluctuations as evident from Fig. 4.6 (a). At 200 °C (Fig. 4.6 b), the coefficient of friction for Ni_3Al appears to stabilise after 1300 s whereas for the NI-10A, NI-10W, and NI-10AW stabilisation seems to occur after an initial run-in duration of 1000 s, 800 s and 600 s. There is apparently no run-in period for Ni_3Al at 400 °C while the coefficient of friction stabilises after 200 s for NI-10A, NI-10W and NI-10AW, as seen from Fig. 4.6 (c). The NI-10A composite has shown a relatively large amplitude of fluctuations at 400 °C throughout the period of sliding. At 600 °C and 800 °C (Figs. 4.6 d and e), NI-10A, NI-10W, and NI-10AW have shown an almost steady coefficient of friction for the complete duration of sliding, while the coefficient of friction for NI has been found to stabilise after about 200 s of sliding. One may also observe that NI, NI-10A and NI-10W have relatively large fluctuations in amplitude in comparison to NI-10AW composite. It may also be noticed that NI-10AW has a lower coefficient of friction followed by NI-10W, NI-10A and NI at RT, 200 °C, 400 °C, 600 °C and 800 °C, respectively.

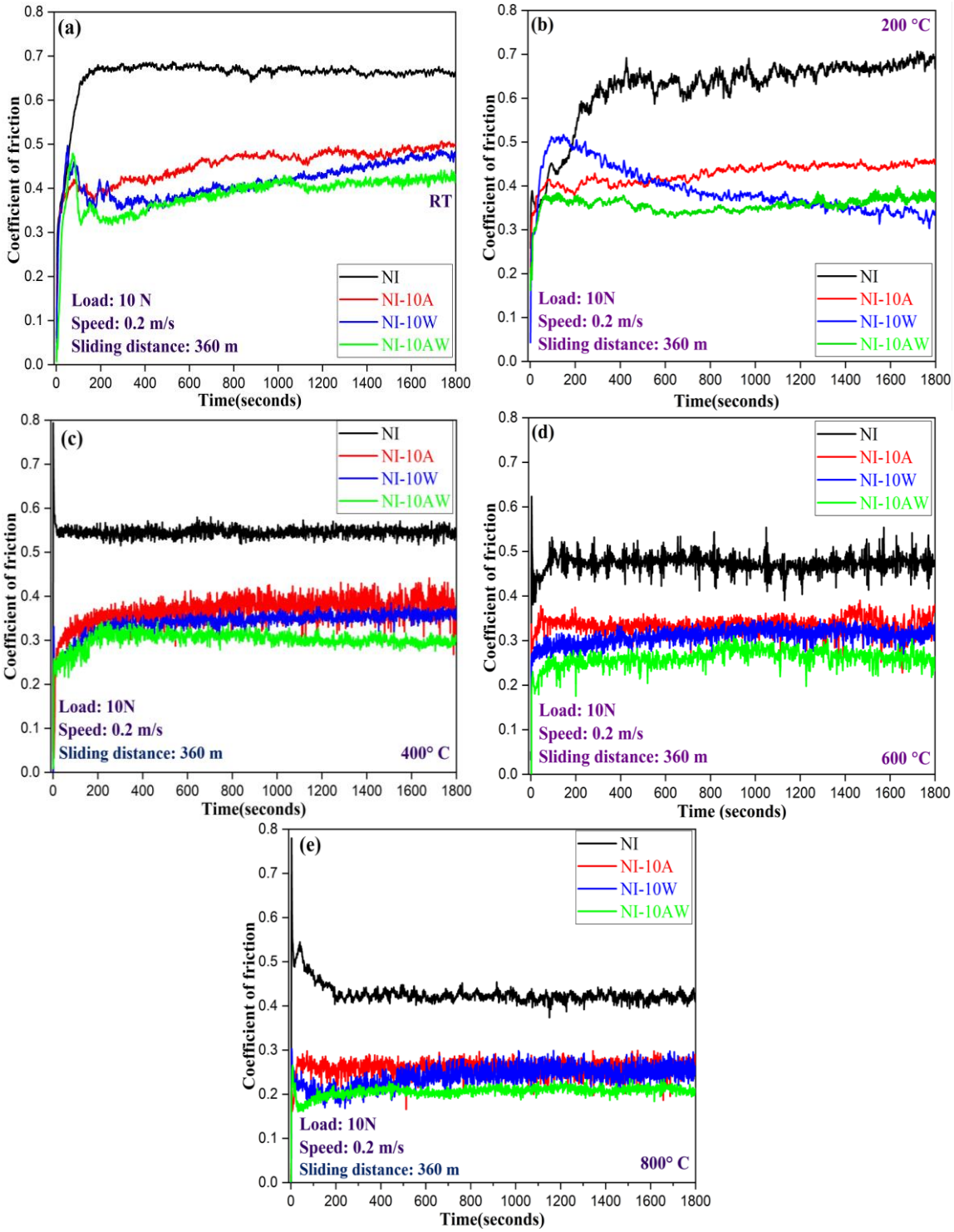

Fig. 4.6: Variation of coefficient of friction with time at (a) RT, (b) 200 °C, (c) 400 °C, (d) 600 °C and (e) 800 °C for the Ni_3Al, Ni_3Al-10Ag, Ni_3Al-10WS_2 and Ni_3Al-5Ag-5WS_2 composite.

4.1.3.1.2 Variation of coefficient of friction with temperature

Figure 4.7 illustrates the variation of the average coefficient of friction with temperature for all the composites examined in this study, and the average coefficient of friction for

Ni_3Al, Ni_3Al-10Ag, Ni_3Al-10WS_2, and Ni_3Al-5Ag-5WS_2 composite is observed to decrease with increasing temperature from RT to 800 °C. It may be observed that the addition of solid lubricant either Ag or WS_2 brings about a significant reduction in the average coefficient of friction of Ni_3Al over the entire range of temperature used in the investigation. It could also be seen from Fig. 4.7 that the addition of WS_2 is more beneficial for reducing the coefficient of friction in comparison to the same amount of addition of Ag. However, Ni_3Al-5Ag-5WS_2 composite has shown the lowest coefficient of friction at all the test temperatures, indicating the occurrence of a synergetic action between Ag and WS_2 in reducing friction. The value of average coefficient of friction for Ni_3Al-5Ag-5WS_2 is found to decrease from 0.39 to 0.21 as the temperature is raised from RT to 800 °C.

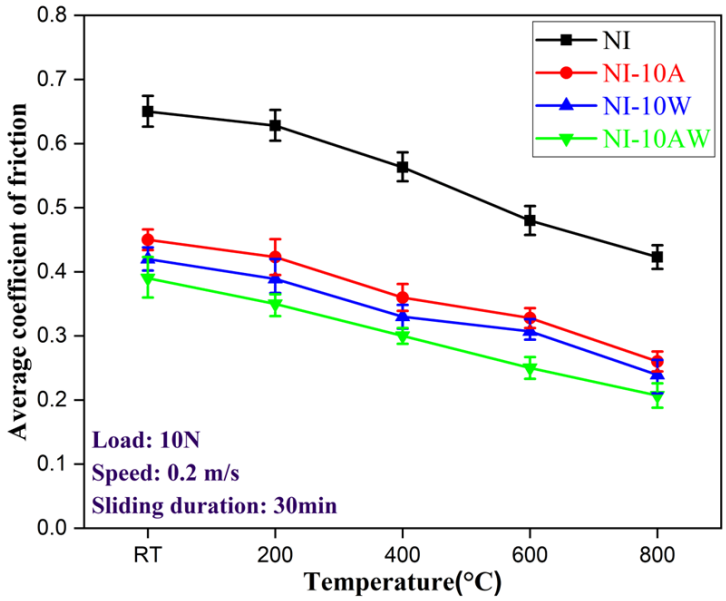

Fig. 4.7: variation of average coefficient of friction with temperature for the Ni_3Al, Ni_3Al-10Ag, Ni_3Al-10WS_2 and Ni_3Al-5Ag-5WS_2 composite.

4.1.3.2 Dry sliding wear

4.1.3.2.1 Variation of wear rate with temperature

The wear rate of Ni_3Al, Ni_3Al-10Ag, Ni_3Al-10WS_2 and Ni_3Al-5Ag-5WS_2 composites as a function of testing temperature from RT to 800 °C is shown in Fig. 4.8. The wear rates of

NI, NI-10A and NI-10W follow a similar pattern with an increase in temperature. The wear rates of NI, NI-10A and NI-10W have been observed to increase from 3.52 to 5.95 x 10^{-5} mm^3/Nm, 2.96 to 6.66 x 10^{-5} mm^3/Nm and 1.582 to 2.52 x 10^{-5} mm^3/Nm, respectively, as the temperature is raised from RT to 400 °C, beyond which the same is found to decrease for the temperatures of 600 °C and 800 °C, as seen from Fig. 4.8. One may observe that the composite NI-10A has shown a lower wear rate than NI at RT, 600 and 800 °C whereas the same is higher than NI at the temperatures of 200 and 400 °C as evident from Fig. 4.8. The composite containing WS_2 has been observed to show a consistently lower wear rate in comparison to both NI and NI-10A over the entire temperature range. The wear rate for the NI-10AW composite has been observed to decrease with increasing temperature from RT to 800 °C, and it has shown the lowest wear rate among all materials examined in the current study, reflecting the combined effectiveness of Ag and WS_2 in diminishing wear.

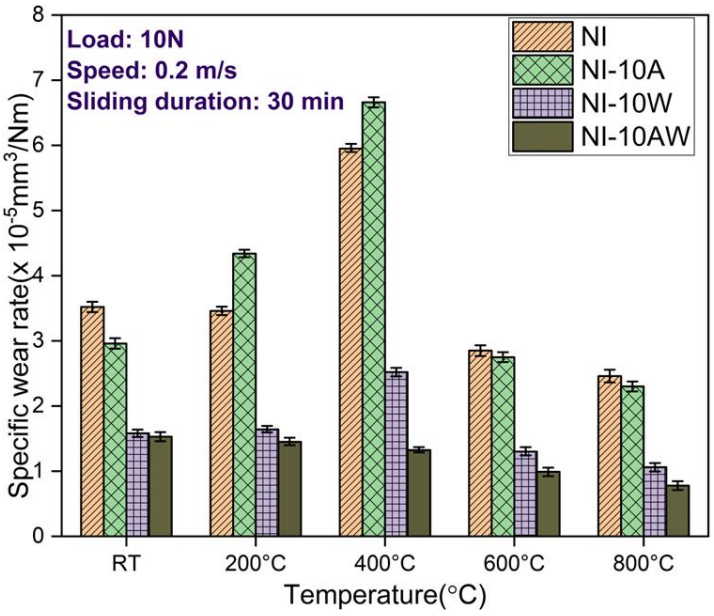

Fig. 4.8: Variation of wear rates with temperature for the Ni_3Al, Ni_3Al-10Ag, Ni_3Al-10WS_2 and Ni_3Al-5Ag-5WS_2 composite.

4.1.4 Morphology of worn surfaces

4.1.4.1 Field emission scanning electron microscopy of worn composites and counterface ball

The FESEM micrographs of worn surface of Ni_3Al (NI) and corresponding Si_3N_4 ball after sliding at RT, 200 °C, 400 °C, 600 °C and 800 °C are shown in Figs. 4.9 (a-g) and 4.10 (a-g) respectively. At RT (Fig. 4.9 a), the worn surface of Ni_3Al shows the presence of loose wear particles apart from a patchy transfer layer of wear debris, whereas that worn at 200 °C (Fig. 4.9 b) displays the presence of wear debris and ploughing. At 400 °C (Fig. 4.9 c), the worn surface displays the presence of adhered debris and grooves in the direction of sliding apart from some delamination. The worn track of NI at 600 °C (Fig. 4.9 d) reveals the presence of a well-compacted transfer layer containing oxides of Ni and Mo as indicated by the presence of oxygen in the EDS analysis given in Fig. 4.9 (e) along with signs of delamination at a few locations. However, a smooth and compacted transfer layer containing oxides of Ni and Mo, as indicated by the presence of oxygen in the EDS analysis given in Fig. 4.9 (g), is observed at 800 °C covering almost the entire worn track with no visible grooves as seen from Fig. 4.9 (f). The presence of a smooth tribo-layer over the worn surface of NI at 600 °C and 800 °C (Figs. 4.9 d and f) might have resulted in a lower coefficient of friction and wear rate in comparison to 400 °C (Fig. 4.9 c), 200 °C (Fig. 4.9 b) and RT (Fig. 4.9 a). The worn surface of the silicon nitride (Si_3N_4) ball at 600 °C (Fig. 4.10 d) and 800 °C (Fig. 4.10 f) confirms the presence of the material transferred from the composite (as revealed by EDS analysis shown in Figs. 4.10 e and g). The transferred material appears to have formed a transfer layer over the Si_3N_4 ball surface with different extent of area coverage and degree of compaction depending on the temperature. However, the layer is seen to be more compact and smoother at 600 °C and 800 °C.

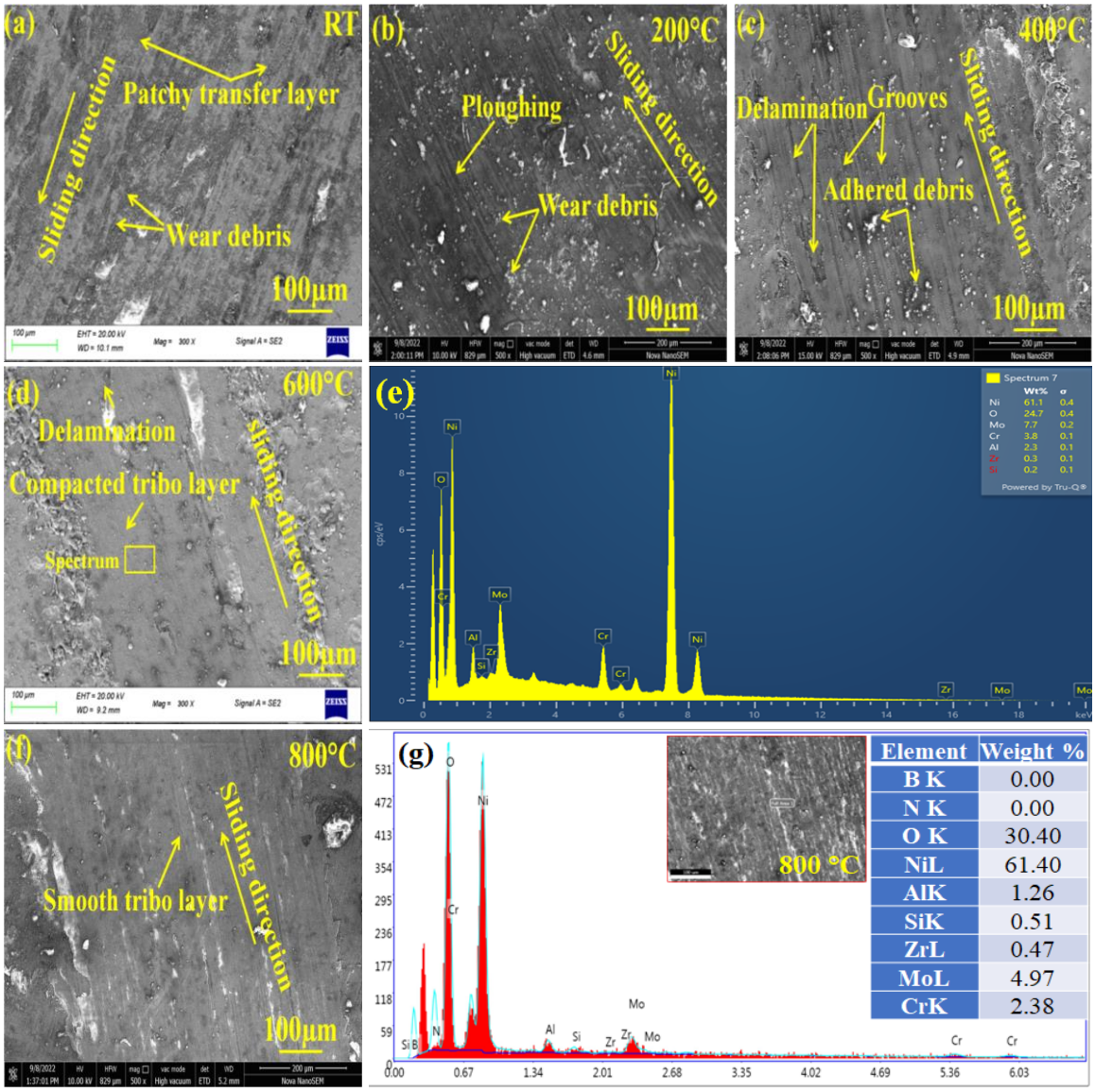

Fig. 4.9: FESEM micrographs of the worn-out Ni_3Al composite at (a) RT (b) 200 °C (c) 400 °C (d) 600 °C (f) 800 °C, and EDS analysis of worn NI at 600 °C and 800 °C (e and g).

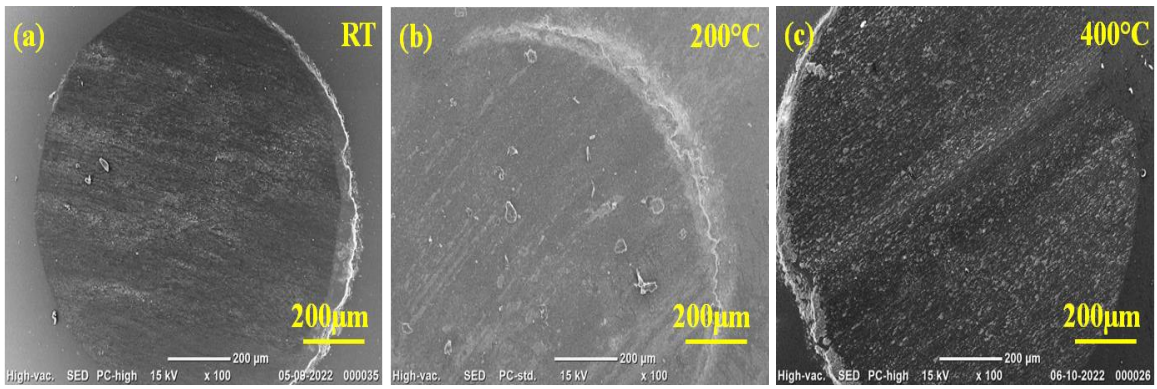

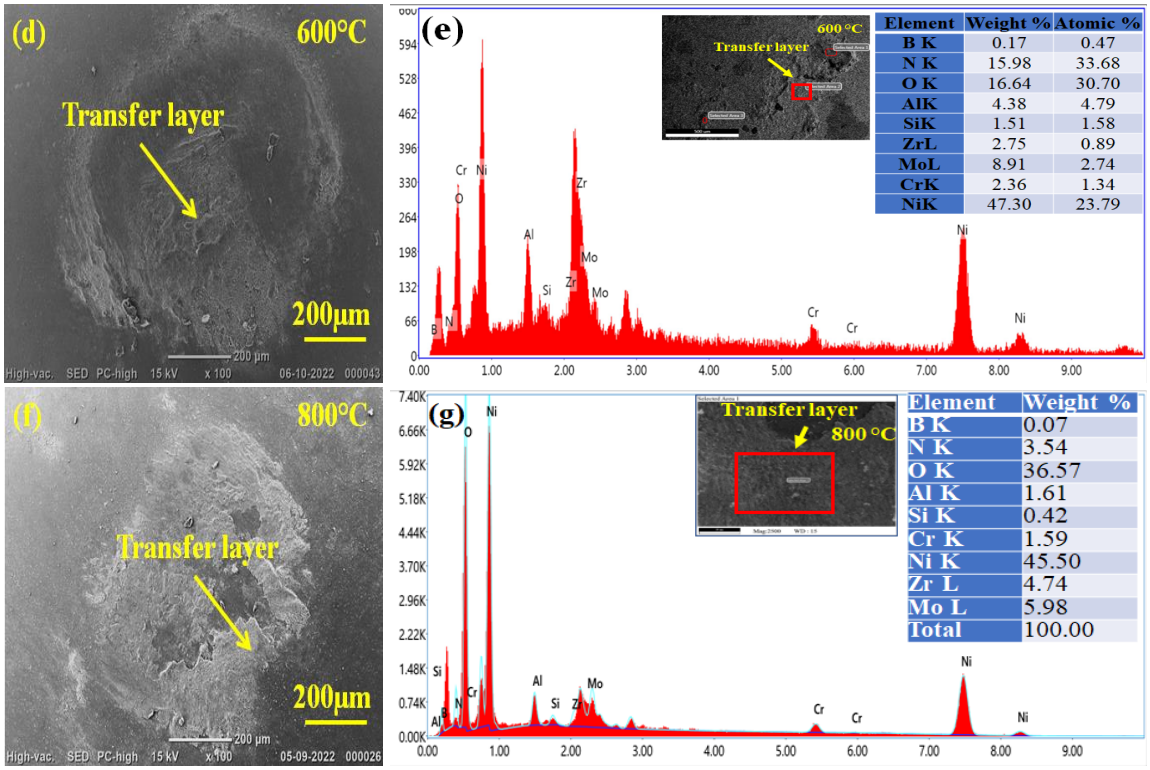

Fig. 4.10: FESEM micrographs of the worn-out silicon nitride ball (counterface) (a) RT (b) 200 °C (c) 400 °C (d) 600 °C (f) 800 °C, and EDS analysis of worn Si_3N_4 ball at 600 °C and 800 °C (e and g).

Figures 4.11 (a-h) and 4.12 (a-f) show the morphology of the worn surfaces of NI-10A composite and the counterface Si_3N_4 ball after the tribo-tests at RT, 200 °C, 400 °C, 600 °C and 800 °C, respectively. One may observe the presence of loose wear particles and signs of ploughing at the worn track apart from tribo-layer over the whole surface at RT (Fig. 4.11 a). At 200 °C (Fig. 4.11 b), the worn track of NI-10A exhibits the presence of a patchy transfer layer and wear debris. However, a compacted transfer layer of wear debris could be seen on the worn surface of NI-10A at 400 °C besides ploughing marks as depicted in Fig. 4.11 (c). At 600 °C (Fig. 4.11 d), the worn track indicates the existence of a compacted tribo-layer containing silver, whereas a glazed layer at 800 °C (Fig. 4.11 e) having Ag, as revealed by EDS and elemental mapping (Figs. 4.11 g and h) may have contributed in lowering friction and wear in comparison to 400 °C. The transfer of material from the NI-

10A to the Si_3N_4 ball is evident at all temperatures (Figs. 4.12 (a-e)), with the transferred material forming a compact and continuous layer over the worn surface of the counterface Si_3N_4 ball at higher temperatures (600 °C and 800 °C), as confirmed by EDS analysis at 800 °C (Fig. 4.12 f) (transfer layer area marked in Fig. 4.12 e), and the lubricant film containing Ag on the counterface Si_3N_4 ball reduces friction and wear by facilitating easy shearing at the interface.

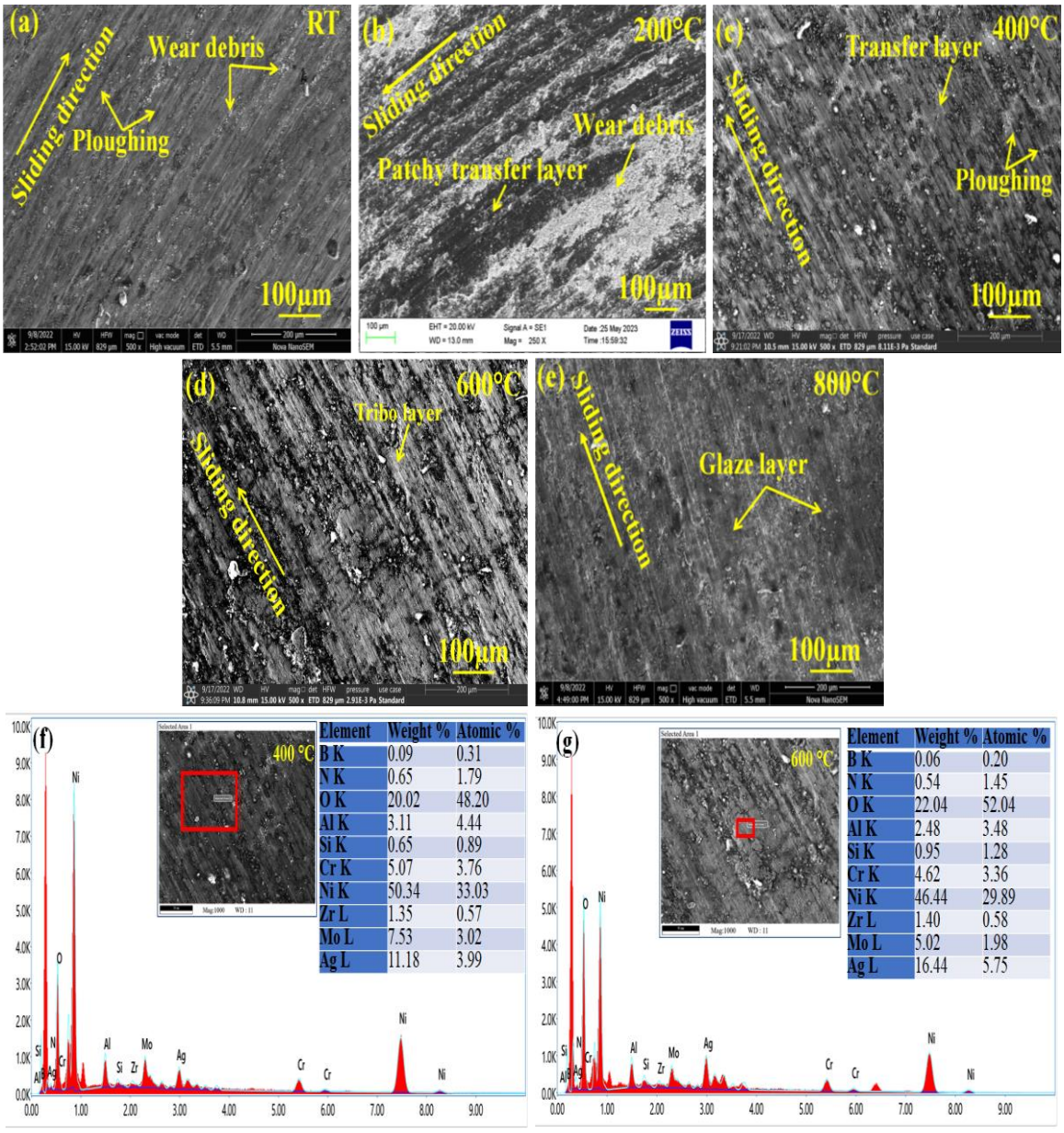

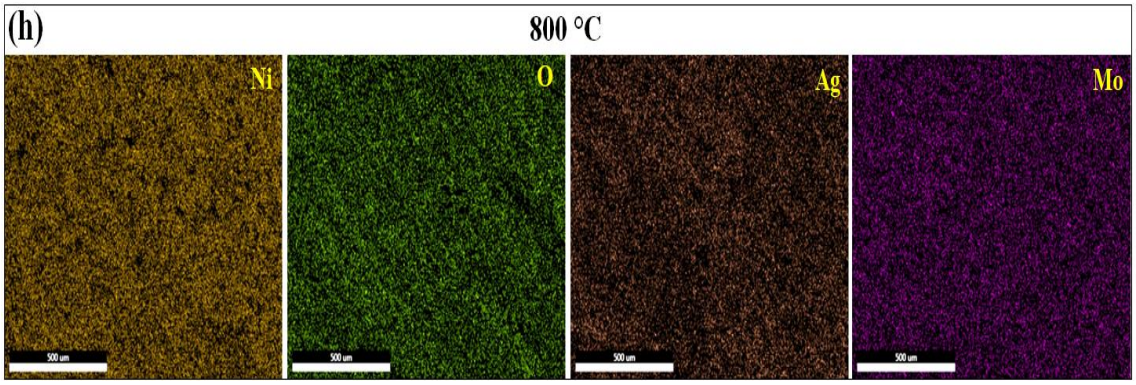

Fig. 4.11: FESEM micrographs of the worn-out Ni_3Al-10Ag composite at (a) RT (b) 200 °C (c) 400 °C (d) 600 °C (e) 800 °C, and EDS analysis of worn NI-10A at 400 °C and 600 °C (f and g) as well as area elemental mapping of Ni, O, Ag and Mo at 800 °C (h).

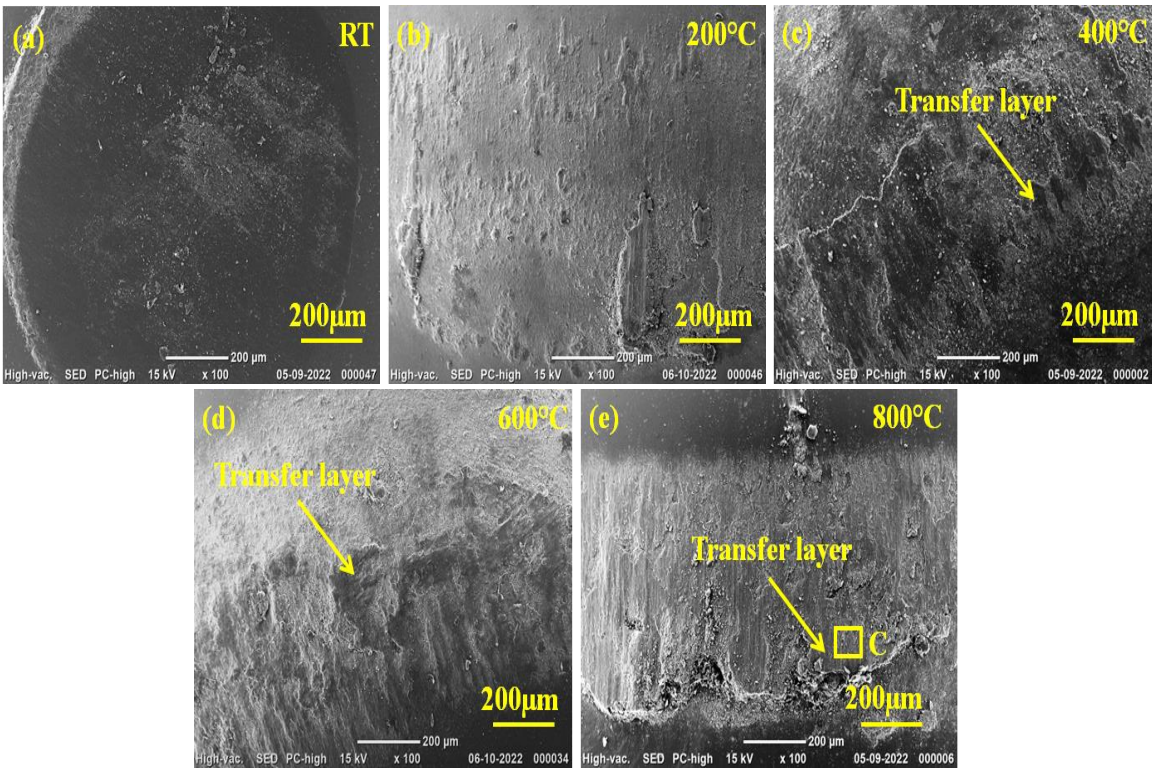

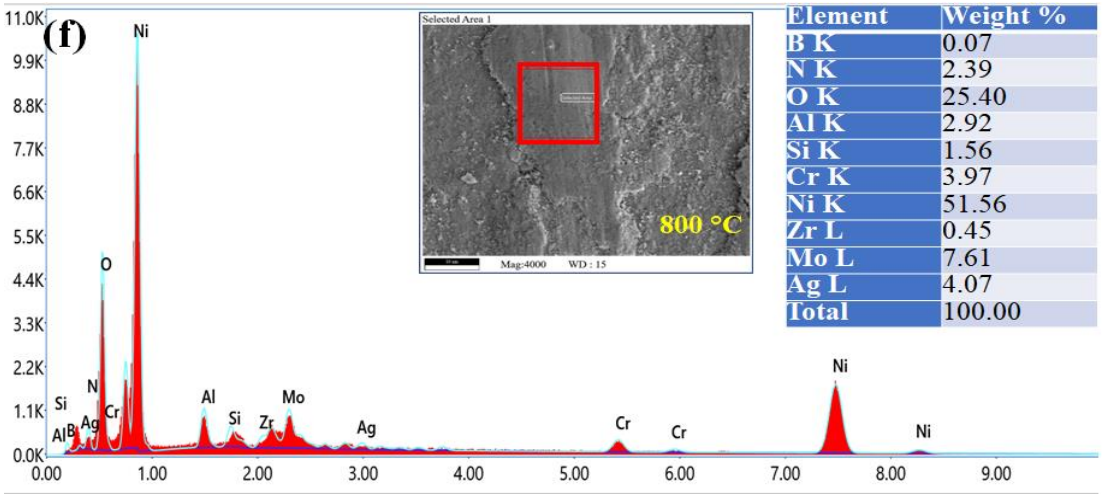

Fig. 4.12: FESEM micrographs of the worn-out silicon nitride ball (counterface) (a) RT (b) 200 °C (c) 400 °C (d) 600 °C (e) 800 °C and its EDS analysis.

Figures 4.13 (a to e) and 4.14 (a to e) illustrate FESEM micrographs of worn track of NI-10W composite and counterface Si_3N_4 balls slid against them at RT, 200 °C, 400 °C, 600 °C and 800 °C, respectively. At RT (Fig. 4.13 a), the worn track shows signs of fine wear marks running parallel to the sliding direction, suggesting abrasive wear events, whereas the worn track at 200 °C (Fig. 4.13 b) shows the presence of wear marks and delamination. The worn track at 400 °C (Fig. 4.13 c) shows the presence of ploughing along with delamination, whereas at 600 and 800 °C the worn surface reveals the presence of a smooth and compacted tribo-layer with no indication of grooves and ploughing (Figs. 4.13 d and e) indicating oxidation as predominant wear mechanism. The presence of oxides has been confirmed by an EDS scan of a selected spot and area on the worn track of composite at 800 °C, as shown in Fig. 4.13. The transferred material from the NI-10W composite to the counterface Si_3N_4 ball (Figs. 4.14 c, d and e), as confirmed by the EDS analysis of the selected area marked in Fig. 4.14 (e), is seen to have formed a transfer layer over the ball surface but with a different area of coverage and degree of compaction, as stated earlier.

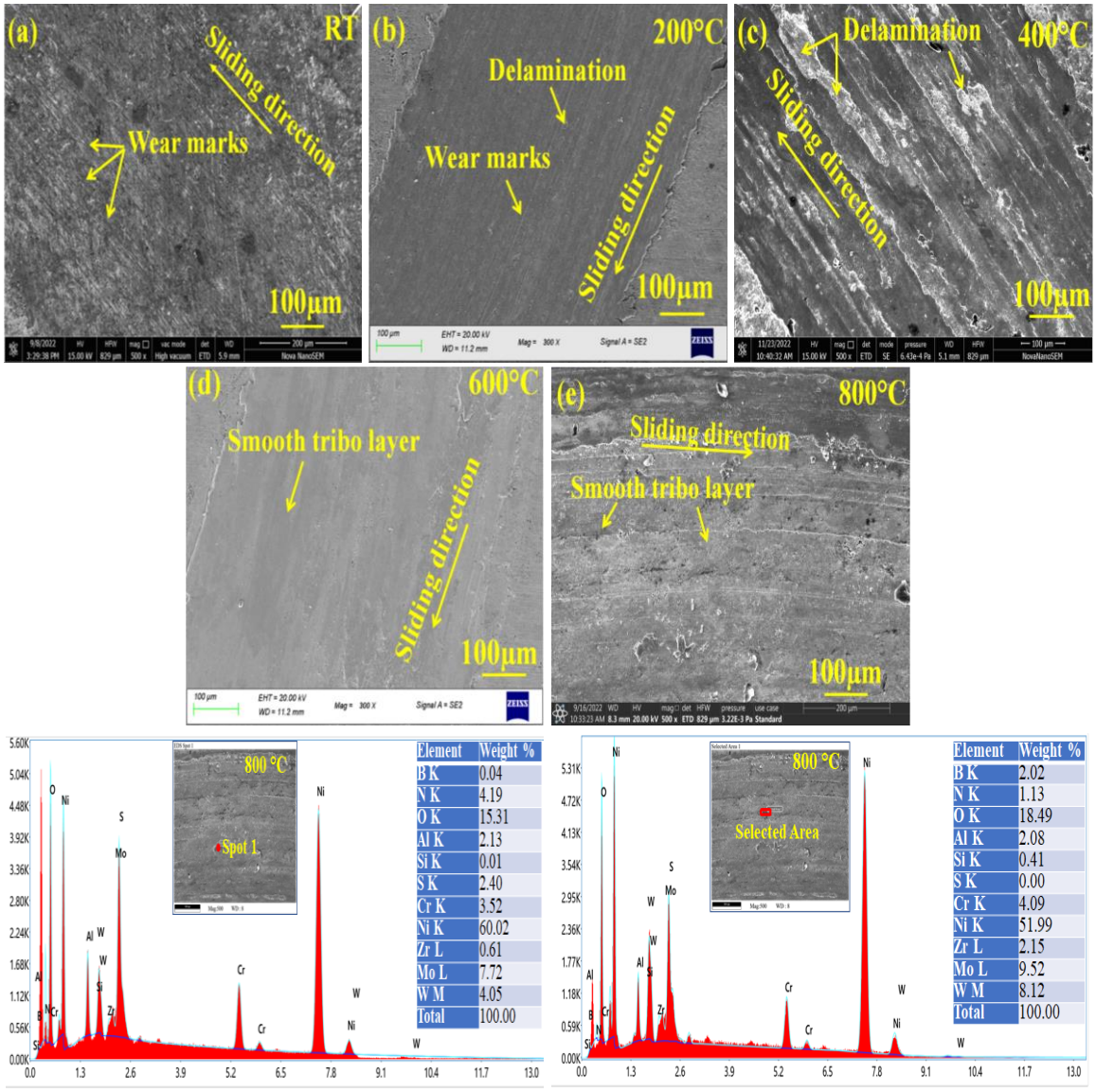

Fig. 4.13: FESEM micrographs of the worn-out Ni_3Al-10WS_2 composite at (a) RT (b) 200 °C (c) 400 °C (d) 600 °C (e) 800 °C and its EDS analysis.

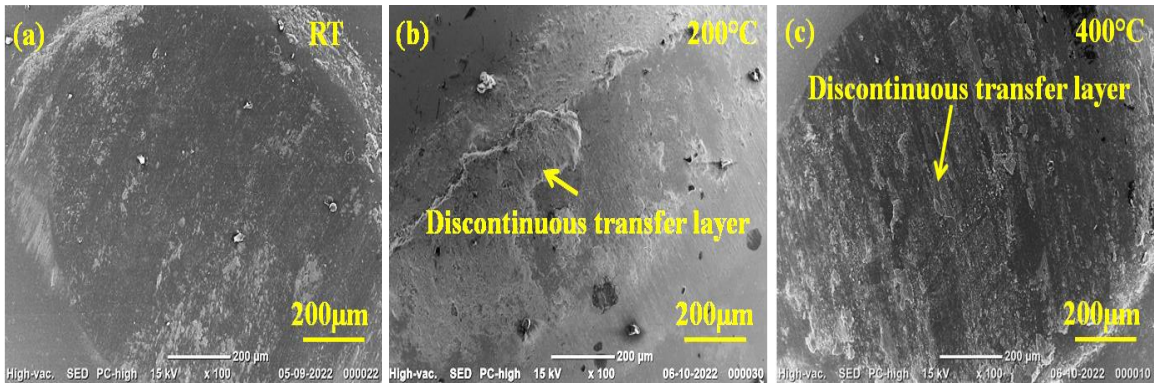

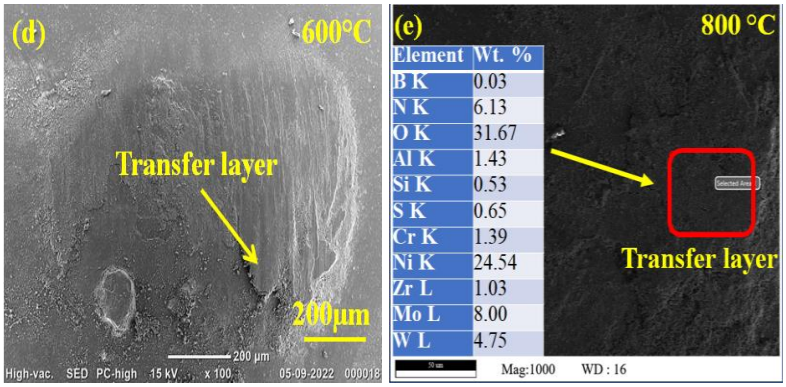

Fig. 4.14: FESEM micrographs of the worn-out silicon nitride ball (counterface) (a) RT (b) 200 °C (c) 400 °C (d) 600 °C (e) 800 °C and its EDS analysis.

Figures 4.15 (a-e) and 4.16 (a-e) demonstrate the morphology of worn surfaces of NI-10AW composite and the corresponding Si_3N_4 counterface balls at RT, 200 °C, 400 °C, 600 °C and 800 °C, respectively. One may observe the presence of loose wear debris and grooves at the worn track apart from the loose transfer layer over the entire surface at RT (Fig. 4.15 a). At 200 °C (Fig. 4.15 b), the worn track of the NI-10AW composite exhibits the presence of wear debris, sliding marks and tribo-layer. However, fine wear particles and a relatively well-compacted transfer layer of wear debris could be seen on the worn surface of NI-10AW at 400 °C, besides ploughing marks, as depicted in Fig. 4.15 (c). At 600 °C (Fig. 4.15 d), the worn track indicates the existence of a compacted tribo-layer as well as delamination, whereas at 800 °C (Fig. 4.15 e), the worn surface shows the presence of a smooth and compacted tribo-layer along with glazed layer comprised of Ni, Ag, W, Mo, and O elements as revealed by the elemental map of worn tack at 800 °C as seen in Fig. 4.15. It has been observed that most of the worn surface of NI-10AW composite and counterface Si_3N_4 ball is covered with Ni, Ag, W, Mo, and O elements. The transferred material from NI-10AW composite to the Si_3N_4 ball (Figs. 4.16 c, d and e), as confirmed by elemental mapping and EDS analysis of the worn surface at 800 °C (Fig. 4.16 e) and depicted in Fig. 4.16, is seen to have formed a transfer layer over the counterface Si_3N_4 ball with a different area of coverage and degree of compaction.

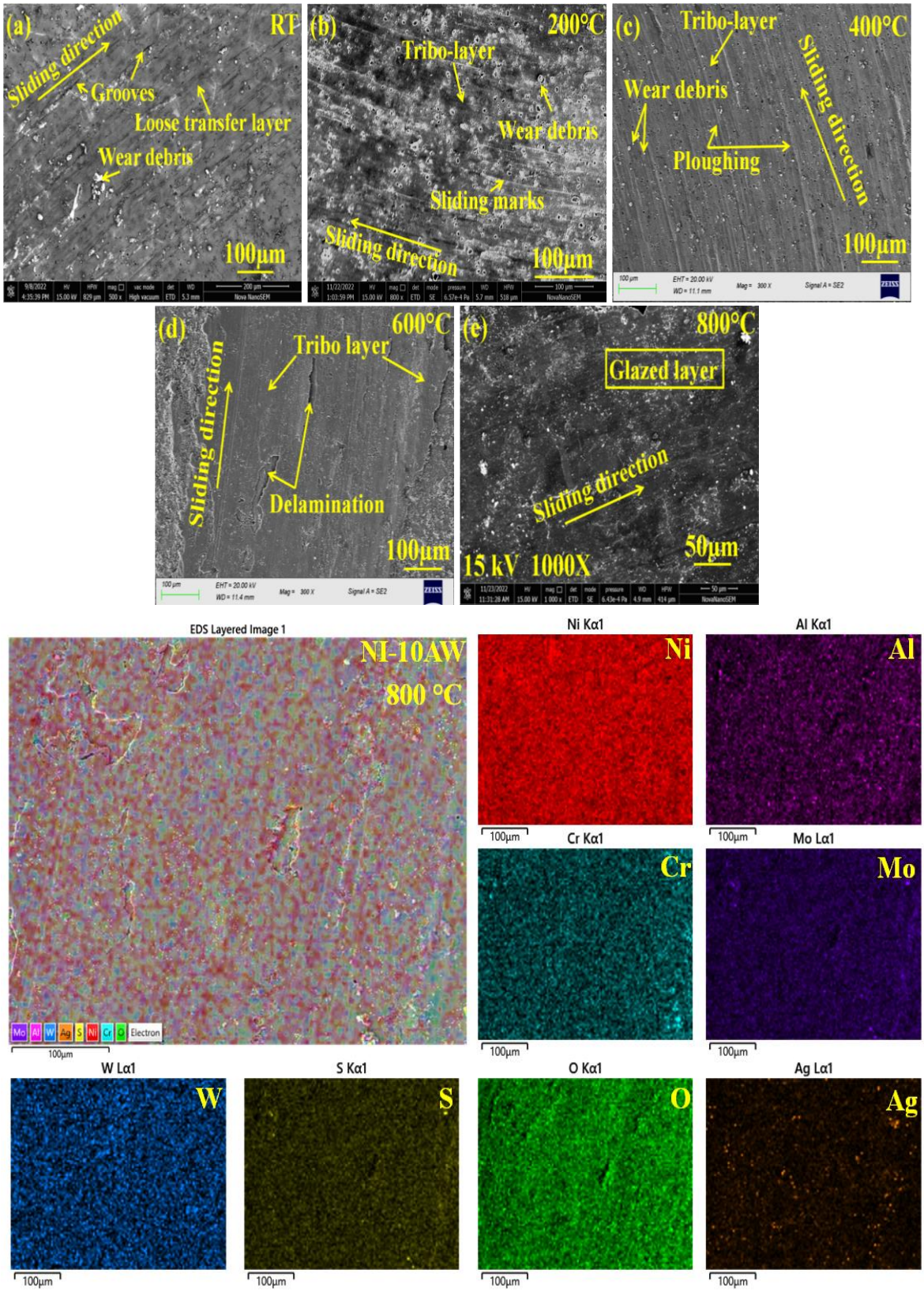

Fig. 4.15: FESEM micrographs of the worn-out Ni_3Al-5Ag-5WS_2 composite at (a) RT (b) 200 °C (c) 400 °C (d) 600 °C (e) 800 °C along with the corresponding area elemental mapping of Ni, Al, Cr, Mo, W, S, O and Ag.

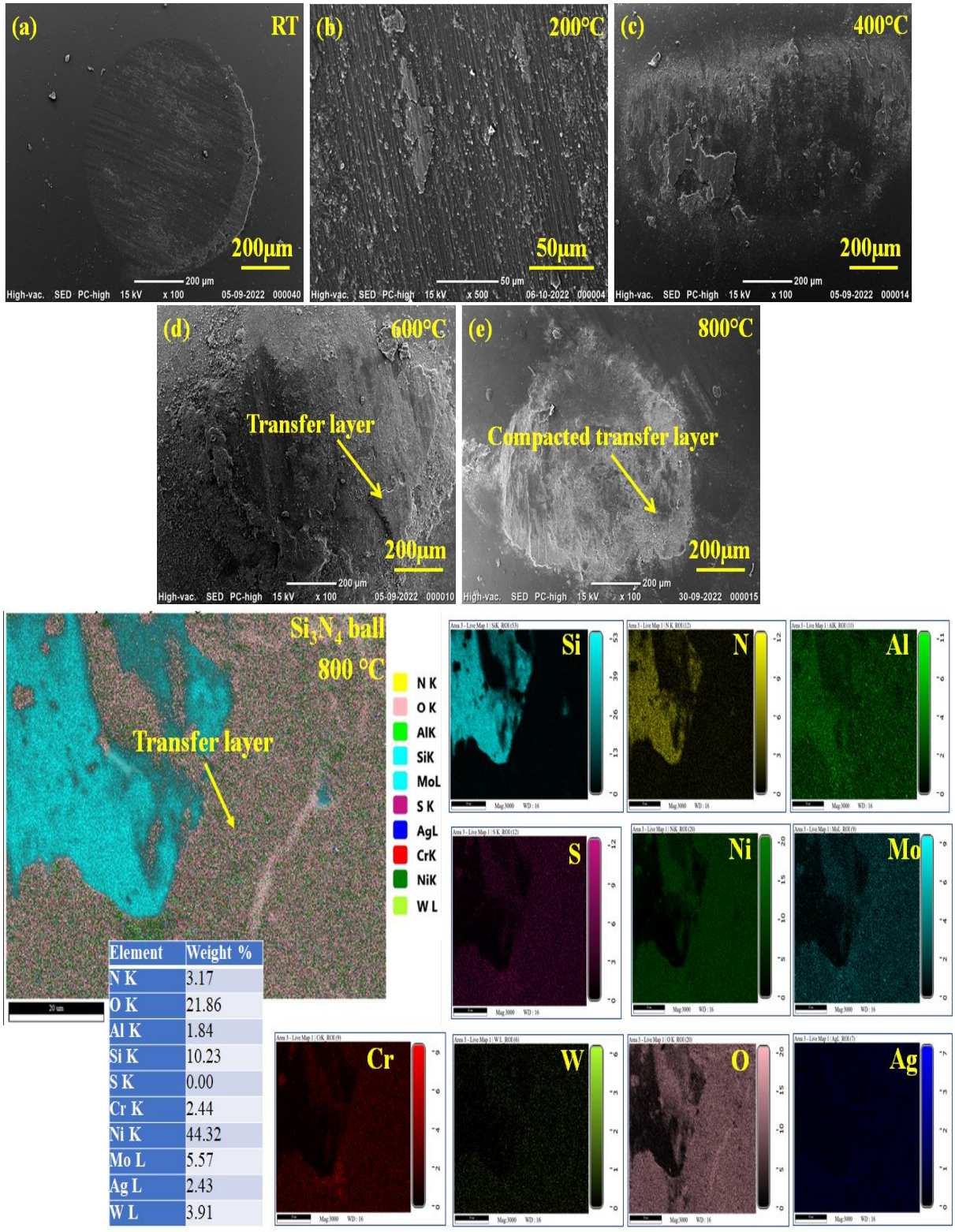

Fig. 4.16: FESEM micrographs of the worn-out Si_3N_4 ball (counterface) (a) RT (b) 200 °C (c) 400 °C (d) 600 °C (e) 800 °C along with the corresponding area elemental mapping of Si, N, Al, S, Ni, Mo, Cr, W, O and Ag.

4.1.4.2 X-ray diffraction analysis of worn surface of composites

The X-ray diffraction patterns of worn NI, NI-10A, NI-10W and NI-10AW composites at various temperatures used in the current work are shown in Figs. 4.17 (a to d). XRD pattern of worn surface of NI (Fig.4.17 a) reveals the formation of Ni_3Al (ICSD 03-065-0430) at RT, Ni_3Al (ICSD 03-065-0430), MoO_3 (ICSD 00-021-0569), and $NiMoO_4$ (ICSD 00-045-142) at 200 °C. However, at 400 °C, 600 °C and 800 °C, a new compound corresponding to NiO (ICSD 01-089-7130), apart from MoO_3 and $NiMoO_4$ could be observed, whereas at 800 °C, MoO_3 peak disappeared. Fig. 4.17 (b) shows the presence of peaks of Ni_3Al and Ag (ICSD 01-087-0598) at room temperature, whereas additional peaks of NiO, MoO_3 and $NiMoO_4$ are also observed at 400 °C. However, at 600 °C and 800 °C, new peaks corresponding to $Ag_2Mo_2O_7$ (ICSD 00-021-1339) and Ag_2MoO_4 (ICSD 00-008-473) could be observed. Fig. 4.17 (c) corresponding to NI-10W composite shows the presence of Ni_3Al and WS_2 (ICSD 01-084-1399) at RT and 200 °C whereas additional peaks of MoO_3, $NiMoO_4$ are also observed at 200 °C. However, at 400 °C, a new diffraction peak corresponding to NiO, whereas at 600 °C and 800 °C, new peaks corresponding to WO_3 (ICSD 01-088-0550) could be observed apart from NiO and $NiMoO_4$. The XRD pattern of the worn surface of NI-10AW composite given in Fig. 4.17 (d) reveals the presence of peaks corresponding to Ni_3Al at RT to 200 °C, Ag at RT to 800 °C, WS_2 at RT to 400 °C, MoO_3 at 200 °C to 600 °C and $NiMoO_4$ at 800 °C whereas peaks corresponding to WO_3, Ag_2MoO_4 and $Ag_2Mo_2O_7$ at 600 °C to 800 °C could be observed.

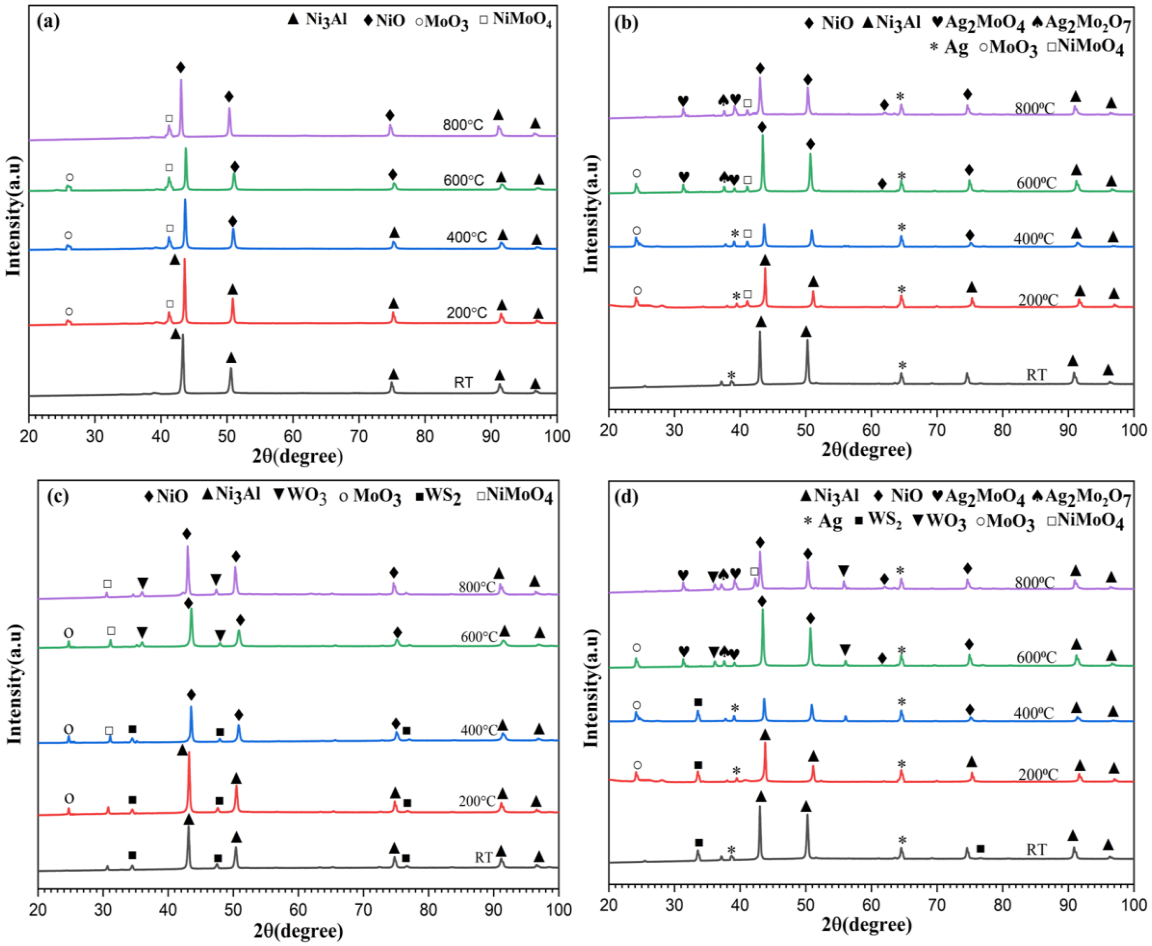

Fig. 4.17: X-ray diffraction patterns of worn composite (a) Ni_3Al, (b) Ni_3Al-10Ag, (c) Ni_3Al-10WS_2, and (d) Ni_3Al-5Ag-5WS_2 at various temperatures.

4.1.4.3 Raman spectroscopy of worn surface of composites

The micro-Raman spectrum of the worn NI, NI-10A, NI-10W and NI-10AW composites at different test temperatures are presented in Figs. 4.18 (a-d). On the worn track of the NI composite, peaks corresponding to NiO, MoO_3 and $NiMoO_4$ were identified at 400°C, 600 °C and 800 °C (Fig. 4.18 a), respectively. The peaks corresponding to NiO, $NiMoO_4$, MoO_3 and Ag_2MoO_4 could be observed at 400 °C, 600 °C, and 800 °C, and $Ag_2Mo_2O_7$ observed at 600 °C and 800 °C (Fig. 4.18 b). Raman spectra of the worn track of NI-10W composite reflect the presence of NiO, WO_3, MoO_3 and $NiMoO_4$ peaks at 400 °C, 600 °C, and 800 °C (Fig. 4.18 c). However, the peaks corresponding to NiO, WO_3, MoO_3, $NiMoO_4$ and Ag_2MoO_4 phases were present on the worn track of NI-10AW composite at 400 °C, 600

°C, and 800 °C, and $Ag_2Mo_2O_7$ at 600 °C and 800 °C as depicted in Fig. 4.18 (d). Beyond 400 °C, Ag_2MoO_4 probably forms on the worn track because of a tribo-chemical reaction. It has been reported that at elevated temperatures, molybdates of silver (Ag_2MoO_4 and $Ag_2Mo_2O_7$), NiO, MoO_3, WO_3 and $NiMoO_4$ offer effective lubrication by forming an easy-to-shear interface [25,27,130,131].

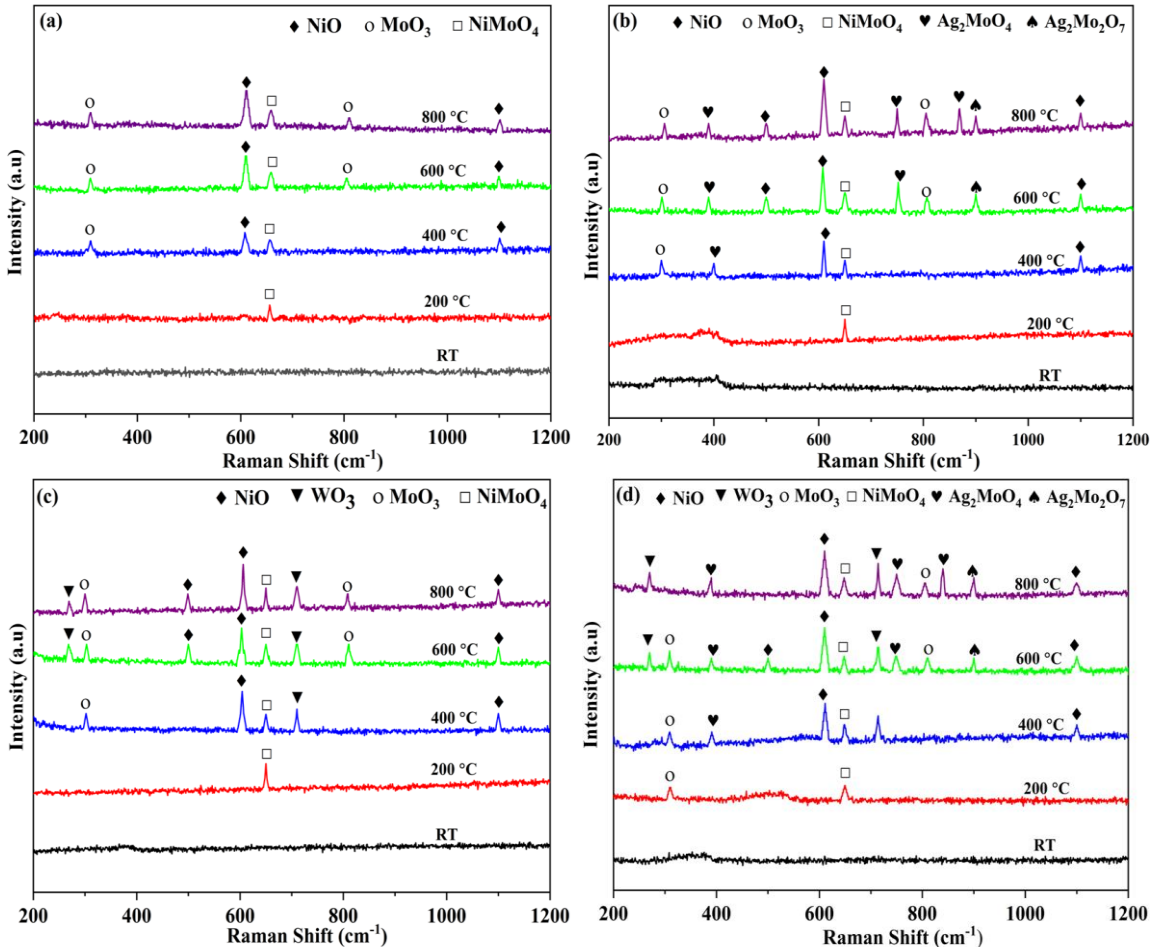

Fig. 4.18: Raman spectra of worn composite (a) Ni_3Al, (b) Ni_3Al-10Ag, (c) Ni_3Al-10WS_2, and (d) Ni_3Al-5Ag-5WS_2 at various temperatures.

4.1.4.4 Examination of subsurface

The FESEM micrographs in Fig. 4.19 depict the cross-section and thickness of oxide layers for NI, NI-10A, NI-10W, and NI-10AW at 800 °C, which reveal that the presence of a glaze layer at NI-10AW (Fig. 4.19 d) is thicker (16.09 μm) than the layers at NI-10W (9.457 μm), NI-10A (6.95 μm) and NI (2.22 μm). This analysis is consistent with the results of XRD

(Fig. 4.17 d) and Raman spectra (Fig. 4.18 d), which indicate that relatively more NiO, MoO_3, WO_3, $NiMoO_4$, Ag_2MoO_4, and $Ag_2Mo_2O_7$ are formed in the worn surface of NI-10AW with increasing temperature, resulting in a thicker layer.

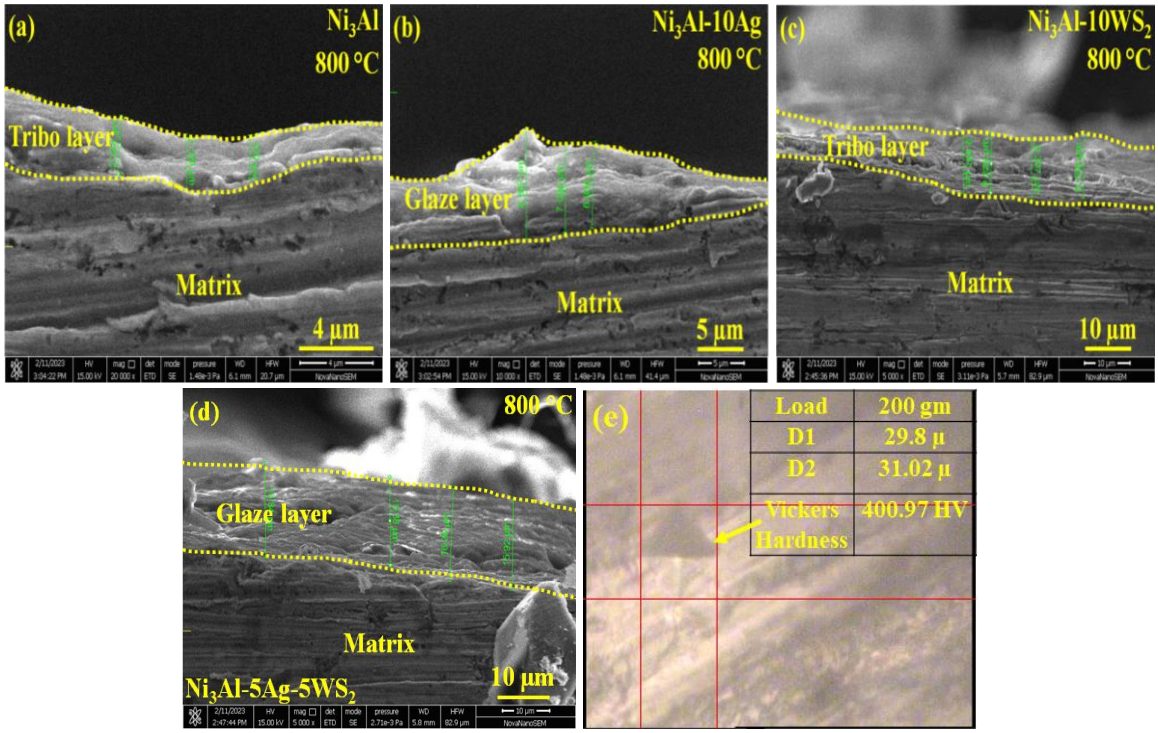

Fig. 4.19: FESEM micrographs of cross-section or subsurface of worn track at 800 °C corresponding to (a) Ni_3Al, (b) Ni_3Al-10Ag, (c) Ni_3Al-10WS_2, and (d) Ni_3Al-5Ag-5WS_2 composites and microhardness of glaze layer on NI-10AW at 800 °C (e).

4.2 Discussions

The incorporation of Ag in Ni_3Al results in the reduction of the hardness of the Ni_3Al-based composite due to the inherent soft nature of silver, as indicated by Zhai et al. [34]. However, the addition of WS_2 brings about an increase in the hardness of the intermetallic compound due to its high hardness, as suggested by an earlier study[132]**.** The effect of combining both Ag and WS_2 (NI-10AW composite) also leads to a marginal reduction in the hardness of base matrix of Ni_3Al, reflecting that the combination of a soft and hard lubricating phase is beneficial in retaining the initial hardness of intermetallic compound, i.e., Ni_3Al.

The variation of coefficient of friction with time has shown a fluctuating trend with minor fluctuations in amplitude for all NI as well as composites, which may be attributed to the initial roughness of the surfaces. As the sliding continues, the surfaces of mating bodies get smoothened and attain better conformity after a short run-in period, beyond which the coefficient of friction stabilises, as evident from Fig. 4.6. The relatively larger fluctuations shown by NI-10A in comparison to NI, NI-10W and NI-10AW may be attributed to its relatively lower hardness which allows the penetration of harder asperities of the hard Si_3N_4 ball causing abrasion despite the presence of Ag.

The variation of coefficient of friction and wear rate with temperature illustrated in Figs. 4.7 and 4.8, respectively, for NI, NI-10A, NI-10W and NI-10AW may be explained based on (i) the presence of loose wear particles, (ii) the nature of transfer layer, i.e., loosely bound or well compacted, continuous or patchy, (iii) the area coverage of transfer layer over the surface and (iv) incidence of oxides or lubricious species present on the worn surfaces of NI and composites and the counterface balls slid against them. The existence of loose wear particles at the sliding interface leads to abrasion, whereas the presence of a loosely bound and discontinuous transfer layer gives rise to direct contact between mating materials, both of which result in relatively higher friction and a larger loss of material. On the other hand, a well-compacted and smooth transfer layer inhibits direct contact between the specimen and the counter-body and helps in lowering down the friction and wear rate.

The presence of loose wear debris, grooves, ploughing and discontinuous transfer layer of wear debris and its delamination at a few positions, as seen in Figs. 4.9 (a to c) corresponding NI at RT, 200 °C and 400 °C may have resulted in a higher friction (Fig. 4.7) as well as wear rate (Fig. 4.8) at these temperatures. However, a decrease in coefficient of friction and wear rate beyond 400 °C, i.e., at 600 °C and 800 °C may be attributed to the presence of a well-compacted and smooth transfer layer over the worn surface of NI (Figs.

4.9 d and f) as well as counterface Si_3N_4 balls (Figs. 4.10 d and f) containing oxides of Ni and Mo, namely, NiO, MoO_3 and $NiMoO_4$ which have been shown to possess a lubricious character [35,131,133–135]. The presence of lubricious oxides has been confirmed by the EDS, XRD and Raman spectra of NI and shown in Figs. 4.9 (e and g), 4.17 (a) and 4.18 (a), respectively. The manifestation of the transfer layer on the sliding surfaces hinders the direct contact between elements of tribo-pair, whereas the presence of lubricating oxides in the transfer layer provides easy shearing capability at the interface, leading to an improvement in friction and wear performance in terms of reduced coefficient of friction and wear rate.

The decreasing trend of average coefficient of friction with temperature in NI-10A composite may be attributed to the lubricating effect of Ag from RT to 400 °C as it gets diffused to the worn surface and provides easy-to-shear junctions at the sliding interface [32] as seen from Figs. 4.11 (a to c). However, the reduction in coefficient of friction and wear rate beyond 400 °C may be ascribed to the formation of a compacted tribo-layer and glazed layer at 600 °C and 800 °C (Figs. 4.11 d and e), composed of lubricious oxides like NiO, MoO_3, $NiMoO_4$, Ag_2MoO_4 and $Ag_2Mo_2O_7$ as confirmed by XRD (Fig. 4.17 b) and Raman spectra (Fig. 4.18 b). The significant increase in wear rate from RT to 400 °C (Fig. 4.8) may be attributed to the existence of loose wear particles, which may have caused grooves due to abrasive action and discontinuous transfer layer over the worn surface of NI-10A and Si_3N_4 ball as shown in Figs. 4.11 (a-c) and 4.12 (a-c), which might have permitted direct contact between the composite and counterface Si_3N_4 ball, leading to a relatively larger loss of material from the composite**.** The formation of silver molybdate (Ag_2MoO_4) has been reported to be an excellent high-temperature solid lubricant [25,29,136,137] that forms at temperatures above 500 °C hence its presence is visible at 600 and 800 °C (Figs. 4.17 (b) and 4.18 (b)). Elemental mapping (Fig. 11h) of area in Fig.

4.11 (e) and EDS analysis (Fig. 12 f) of selected area marked in Fig. 4.12 (e) also revealed the presence of oxygen along with the presence of other elements indicating the possibility of formation of oxides of Ni, Mo and Ag on surfaces of both the specimen as well as counterface. The presence of a compacted transfer layer containing lubricious oxides on the worn surfaces of mating bodies (Figs. 4.12 d and e) results in a reduced coefficient of friction and wear rate by inhibiting the direct contact between the mating materials and by providing the easy to shear junctions at the interface as explained earlier for NI. One may also notice that the average coefficient of friction of Ni_3Al-10Ag composites is lower than that of N_3Al at all the temperatures despite its lower hardness in comparison to NI, and this reflects the lubricating efficacy of Ag at relatively lower temperatures (RT to 400 °C) and its molybdates at 600 °C and 800 °C. However, a relatively higher wear rate of NI-10A than NI at 200 °C and 400 °C (Fig. 4.8) reveals the dominating effect of hardness over the lubricating ability of Ag and the inability to form a continuous transfer layer on the sliding surface, which allows direct contact between hard asperities of counterface ball and the composite resulting in higher loss of material. However, beyond 400 °C, the presence of a continuous and well-compacted transfer layer hampers the contact between the composite and ball and reduces the wear rate.

The observed behaviour of average coefficient of friction and wear rate with increasing temperature for NI-10W composite illustrated in Figs. 4.7 and 4.8, respectively, may again be elucidated on the basis of the morphology of the worn surfaces, i.e., the nature of transfer layer, its degree of compaction, and the presence of lubricious species on the composite as well as the ball depicted in Figs. 4.13 and 4.14. A decrease in the average coefficient of friction with increasing temperature (Fig. 4.7) highlights the lubricating capability of WS_2 at low to moderate temperatures (RT to 400 °C), which provides low shear strength junctions at the interface after getting smeared over the worn surface. Similar findings have

also been reported earlier [34]. The increase in wear rate in low-temperature regime (Fig. 4.8) may be due to the absence of a transfer layer at RT (Fig. 4.13 a) or discontinuous transfer layer at 200 °C and 400 °C (Figs. 4.13 b and c) on the NI-10W composite surface and corresponding Si_3N_4 counterface ball surface (Figs. 4.14 a, b and c) and its delamination at several places which might have raised the possibility of direct contact of mating bodies resulting in relatively more material loss. However, a decrease in coefficient of friction as well as wear rate as beyond 400 °C, i.e., at 600 °C and 800 °C may be attributed to the formation of a smooth and compacted transfer layer over the worn surface of composite (Figs. 4.13 d and e) and Si_3N_4 ball (Figs. 4.14 d and e) containing lubricious species namely NiO, WO_3 [34,35], MoO_3 and $NiMoO_4$ as confirmed by the EDS, XRD and Raman spectra of NI-10W as illustrated in Figs. 4.13, 4.17 (c) and 4.18 (c). The relatively lower coefficient of friction and wear rate shown by NI-10W than those observed for NI-10A may be attributed to the higher hardness of NI-10W in comparison to NI-10A.

A continuously decreasing coefficient of friction and wear rate with increasing temperature shown by NI-10AW composite as depicted in Figs. 4.7 and 4.8 may be attributed to the presence Ag and WS_2 on the worn surface of NI-10AW at RT, 200 °C and 400 °C (Figs. 4.15 a-c), which have been reported to function well as lubricants up to 450 °C and 500 °C [33,138]. However, a decrease beyond 400 °C may be attributed the formation of compacted tribo-layer and glaze layer over the worn surface of NI-10AW at 600 °C and 800 °C (Figs. 4.15 d and e) containing lubricious oxides namely, NiO, WO_3, MoO_3, $NiMoO_4$, Ag_2MoO_4 and Ag_2MoO_7 as confirmed by the XRD (Fig. 4.17 d) and Raman spectra (Fig. 4.18 d). It has been indicated that Ag_2MoO_4 and $Ag_2Mo_2O_7$ form at elevated temperatures and have a layered structure of Ag_2O and MoO_3 layers with a silver layer in between, which makes them exceptionally good lubricants at elevated temperatures [60,139]. The elemental mapping of the worn surfaces of NI-10AW (Fig. 4.15 e) and Si_3N_4

ball (Fig. 4.16 e) at 800 °C, as illustrated in Figs. 4.15 and 4.16 also revealed the presence of Ni, Mo, W, S, Ag, Al, and Cr, along with O, indicating the formation of lubricious oxides of Ni, Mo, Ag, and W on the worn surfaces of both the specimen and counterface. The observance of a lesser coefficient of friction and wear rate for NI-10AW in comparison to NI-10W over the entire temperature range reflects the effectiveness of the combination of solid lubricants.

Figure 4.20 illustrates the possible tribo-chemical interactions at the interface based on the observed tribological behaviour and examination of worn surfaces of NI, NI-10A, NI-10W, and NI-10AW under FESEM, XRD and Raman spectroscopy along with elemental distribution. At relatively low temperatures of RT to 400 °C, the presence of a patchy layer and loose wear particles on the surface of NI cause a higher coefficient of friction and wear, whereas a continuous layer containing lubricious oxides on the worn surface of NI as well as ball at 600 °C and 800 °C results in a reduction of coefficient of friction and wear rate by hindering direct contact between the mating materials as seen from Fig. 4.20 (a). The occurrence of a tribo-layer rich in Ag provides effective lubrication in NI-10A (Fig. 4.20 b), leading to a reduced coefficient of friction in comparison to NI from RT to 400 °C while the presence of a discontinuous layer and loose wear particle result in an increased wear rate due to the mechanisms stated earlier. However, the presence of a well-compacted and continuous transfer layer along with a glazed layer at 600 °C and 800 °C on the surface of NI-10A, consisting of lubricious oxides like NiO, Ag_2MoO_4, MoO_3 and $NiMoO_4$ and transfer layer over counterface ball (Fig. 4.20 b) enriched with lubricious oxide of Ni, Ag and Mo, improves the friction and wear performance by inhibiting direct contact between mating bodies. A similar mechanism of lubrication and wear prevention prevails in the case of NI-10W with the formation of lubricious oxides of tungsten (WO_3) apart from NiO, MoO_3 and $NiMoO_4$ as illustrated in Fig. 4.20 (c). The NI-10AW composite surface favours

the smooth sliding due to the formation of a tribo-layer containing Ag and WS_2 from RT to 400 °C (Fig. 4.20 d), whereas at 800 °C a glazed layer comprising of NiO, Ag_2MoO_4, $Ag_2Mo_2O_7$, WO_3 and $NiMoO_4$ and transfer layer over counterface ball enriched with lubricious oxides of Ni, Ag, Mo and W help in diminishing the friction and wear reflecting thus the occurrence of a co-operative synergy between Ag and WS_2.

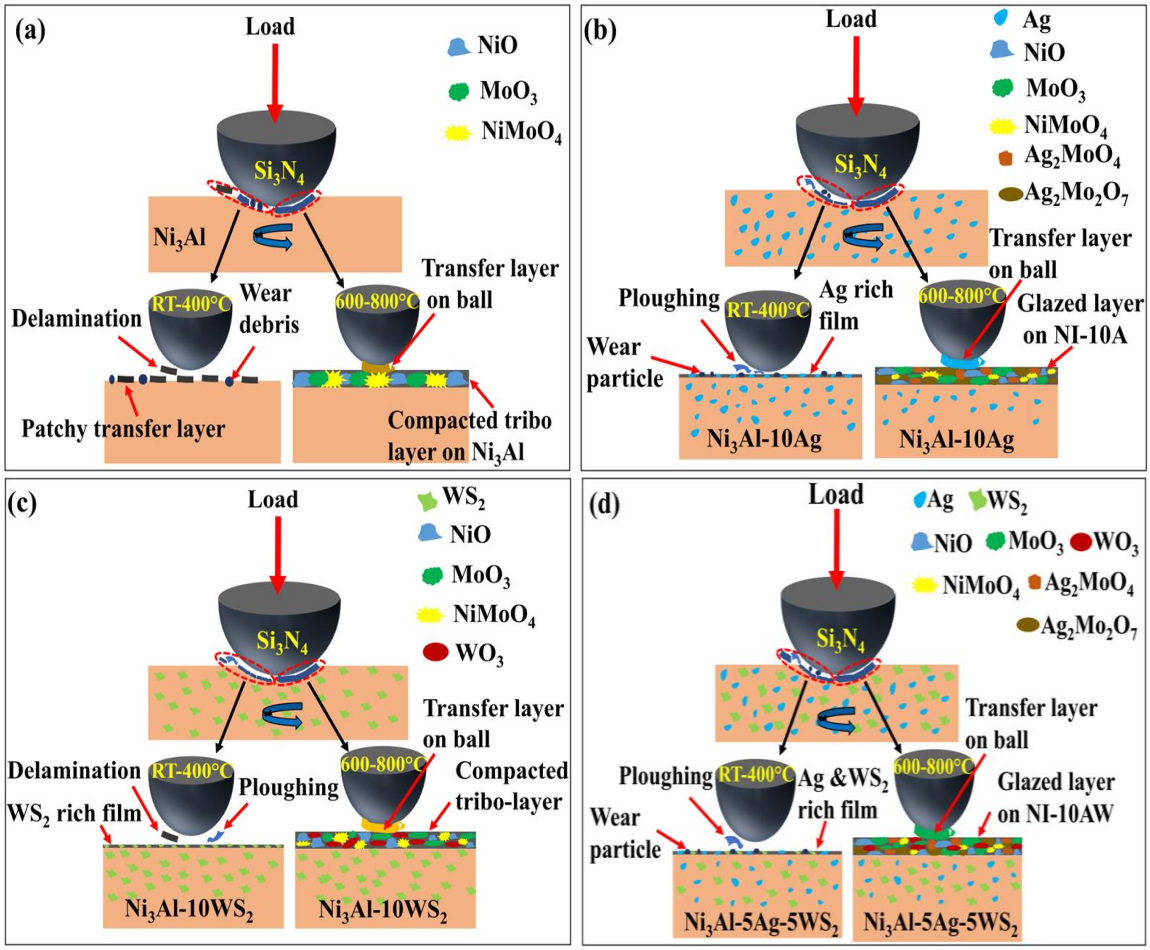

Fig. 4.20: Schematic illustration depicting the wear mechanism of NI, NI-10A, NI-10W and NI-10AW composites.

To summarize, the present investigation on the high-temperature tribological performance of Ni_3Al-based composites containing Ag and WS_2 suggests that the addition of these lubricants either singly or in conjunction is effective in reducing both the coefficient of friction and the wear rate in a range of temperatures from RT to 800 °C. Ni_3Al-5Ag-5WS_2 (NI-10AW) composite has shown the lowest coefficient of friction and the wear rate among

all the materials investigated in the present work, whereas Ni_3Al (NI) has the highest coefficient of friction and wear rate with the exception at RT and 400 °C at which Ni_3Al-10Ag (NI-10A) has the highest wear rate. The coefficient of friction and wear rate observed for Ni_3Al-10Ag and Ni_3Al-10WS_2 (NI-10W) lie in between with Ni_3Al-10WS_2 having slightly lower values. This improved performance of Ni_3Al-5Ag-5WS_2 highlights the occurrence of a synergetic action between Ag and WS_2 in reducing both the friction and wear from RT to 800 °C by overcoming the handicaps of employing a single solid lubricant at a comparable level of hardness of the base intermetallic compound.